UNIVERSITAT POLITÈCNICA DE CATALUNYA
BARCELONATECH
Escola Tècnica Superior d'Enginyeria
de Telecomunicació de Barcelona

STUDY OF BRAIN IMAGING CORRELATES OF MILD COGNITIVE IMPAIRMENT (MCI) AND ALZHEIMER'S DISEASE (AD) WITH MACHINE LEARNING.

A Master's Thesis

Submitted to the Faculty of the

Escola Tècnica d'Enginyeria de Telecomunicació de Barcelona

Universitat Politècnica de Catalunya

by

Anna Canal Garcia

In partial fulfilment

of the requirements for the degree of

MASTER IN TELECOMMUNICATIONS ENGINEERING

Advisor: Veronica Vilaplana Besler

Barcelona, April 2019

Study of brain imaging correlates of Mild Cognitive Impairment (MCI) and Alzheimer's Disease (AD) with machine learning

ANNA CANAL GARCIA

April 17, 2019

Master in Systems, Control and Robotics
School of Electrical Engineering and Computer Science
Master in Telecommunications Engineering
UPC Barcelona School of Telecommunications Engineering

Supervisors: Pawel Herman (KTH), Veronica Vilaplana Besler (UPC)
Examiner: Erik Fransén
Swedish title: Korrelationen mellan lindrig kognitiv störning (MCI) och Alzheimers sjukdom (AD): en maskininlärningsbaserad studie av hjärnbilder

Abstract

Accurate diagnosis in the early stages is an important challenge for the prevention and effective treatment of Alzheimer's Disease (AD). This work proposes a method of analysis of the correlation of Mild Cognitive Impairment (MCI) subtypes and its progression to AD using neuroimages such as structural magnetic resonance imaging (MRI) scans. Basic data pre-processing such as the extraction of brain-tissue related parts of the image, image registration and standardization to the mean and deviation is applied. A convolutional autoencoder (CAE) is used to reduce data dimensionality and learn generic features capturing AD biomarkers, followed by various clustering techniques in order to detect different patterns on MCI data. In addition, six MCI patient clusters are generated based on AD progression information provided by ADNI. The method is evaluated on a total of 1069 structural MRI scans (522 MCI scans, 243 AD scans and, 304 CN scans) on the baseline from ADNI database. No clearly separable clusters are found after using CAE model trained on MCI data. Therefore, it is difficult to confirm a strong correlation between different subtypes of MCI patients and its progression to AD. Nevertheless, a significant correlation within the baseline images of the respective six groups identified based on AD progression is reported. It is hypothesized lack of domain-specific MRI processing, planned in this work, could be a deciding factor about the negative findings in this research.

Sammanfattning

Noggrann diagnos i de tidiga stadierna är en viktig utmaning för förebyggande och effektiv behandling av Alzheimers sjukdom (AD). Detta arbete föreslår en analysmetod av korrelationen mellan subtyper av lindrig kognitiv störning (MCI) och dess progression till AD genom användandet av bildgivande tekniker så som strukturell magnetisk resonanstomografi (MRI). Grundläggande förbehandling som extraktion av hjärnvävnadsrelaterade delar av bilden, bildregistrering och standardisering till medelvärdet och standardavvikelse tillämpas. En faltnings-autoenkoder (CAE) används för att minska datadimensionaliteten och lära sig generiska funktioner som tar bort AD-biomarkörer, följt av olika klusteringstekniker för att upptäcka olika mönster på MCI-data. Dessutom genereras sex MCI-patientkluster baserade på AD-progressions-information tillhandahållen av ADNI. Metoden utvärderades på totalt 1069 strukturella MR-skanningar (522 MCI, 243 AD och 304 CN) på baslinjen från ADNI-databasen. Inga tydligt separerbara kluster finns efter användning av CAE-modell tränad på MCI-data. Det är därför svårt att bekräfta en stark korrelation mellan olika subtyper av MCI-patienter och dess progression till AD. Trots detta rapporteras en signifikant korrelationinom baslinjebilderna för respektive sex grupper som identifierats baserat på AD-progression. Hypotesen är att det saknas domänspecifik MR-behandling, som planerats i detta arbete, skulle kunna vara avgörande för de negativa resultaten i denna forskning.

Resum

El diagnòstic precoç i acurat és un repte important per a la prevenció i el tractament efectiu de la malaltia d'Alzheimer (AD). Aquest treball proposa un mètode d'anàlisi de la correlació dels subtipus de deteriorament cognitiu lleu (MCI) i la seva progressió a AD mitjançant neuroimatges com són les imatges per ressonància magnètica (MRI). S'aplica un pre-processat de dades bàsic com ara l'extracció de parts de la imatge relacionades amb el teixit cerebral, la normalització espacial de les imatges i la normalització respecte a la mitjana i la desviació. S'utilitza un auto-codificador convolucional (CAE) per reduir la dimensionalitat de les dades i aprendre les característiques genèriques que capturen biomarcadors d'AD. Seguidament, s'apliquen diverses tècniques de *clustering* per tal de detectar diferents patrons de dades de pacients MCI. A més a més, es generen sis grups (o *clusters*) de pacients MCI basant-se en la informació de progressió AD proporcionada per ADNI. El mètode és evaluat en un total de 1069 imatges de ressonància magnètica estructural (522 exploracions MCI, 243 exploracions AD i 304 exploracions CN) de la base de dades ADNI les quals corresponen a imatges del primer diagnòstic dels respectius pacients. No es troben *clusters* clarament separables després d'utilitzar el model CAE entrenat amb les dades de pacients MCI. Per tant, és difícil confirmar una forta correlació entre els diferents subtipus de pacients MCI i la seva progressió a AD. No obstant això, es reporta una correlació significant entre les imatges del primer diagnòstic dels sis grups respectius basats en la progressió cap a l'AD. Es planteja la hipòtesi que la manca de processament de domini específic de MRI, ja previst en aquest treball, podria ser un factor decisiu sobre els resultats negatius d'aquesta investigació.

Acknowledgments

I would like to thank my supervisor Pawel Herman who guided me throughout this research, and my friends who has also supervised my work Borja Rodríguez Gálvez, Alexander Aurell and Madita Edeling. I would like to especially thank my lovely Swedish translator Robin Fransson, tack för din hjälp och din stöd. Thanks to my friends from both master degrees, KTH and UPC, to share this learning trip and share insightful discussions. Gràcies a en Lucas per ser el millor referent en aquesta doble titulació. Gràcies a la meva família i a les meves amigues per tot l'amor, comprenssió, suport i paciència al llarg dels anys viscuts.

Contents

Chapter 1

Introduction

Alzheimer's disease (AD), an irreversible neurodegenerative disorder characterized by progressive memory loss and cognitive impairment, is expected to double during the next 20 years due to the increasing life expectancy [1]. AD is the most common type of dementia and currently there is no cure for it. However, the possibility of an effective treatment to delay its progression, especially if diagnosed at an early stage, generates new clinical AD research challenges. One of the most important challenges is to obtain an accurate diagnosis of AD during life, which is based on the presence of cognitive deficits in two or more domains severe enough to interfere with normal daily functioning [1]. It becomes clearer that one should focus on the diagnosis and prognosis in the very early stages when any intervention would have the biggest impact.

The interest to characterize the earliest symptoms of the neurodegenerative process that is likely to convert to AD led to the concept of mild cognitive impairment (MCI), which represents the transitional zone between normal ageing or normal control (NC) and AD. MCI refers to a group of subjects who have some cognitive impairment but of insufficient severity to constitute dementia [2]. There are four categories of MCI: amnestic single and multiple domain, non-amnestic single and multiple domain [3]. MCI, and normally amnestic subtypes, is considered as the prodromal phase of AD. However, not all MCI patients progress to AD. Some of them remain stable for several years, some progress to another dementia and others even improve.

There are several studies [4, 5, 6, 7, 8, 9] which predict the conversion from MCI to AD and thus distinguish stable MCI (sMCI) from progres-

sive MCI (pMCI). The most common approach consists in group comparisons of grey matter (GM) volumes based on magnetic resonance imaging (MRI) in restricted cortical areas [4]. More recently, diffusion tensor imaging (DTI), an imaging technique which provides information on the integrity of white matter (WM) tracts [10], has also been employed [4].
In recent years, measurements of structural changes based on brain MRI scans have been used in order to classify AD patients versus cognitively normal (CN) subjects and to predict the risk of evolution from MCI to AD. Machine learning techniques such as principal component analysis (PCA), linear discriminant analysis (LDA), regression models, support vector machine (SVM) and artificial neural networks (ANNs) have been successfully applied to both structural and functional neuroimaging data for this prediction [7, 11, 12, 13, 8]. Lately, deep learning networks, such as Convolutional Neural Networks (CNNs), have been used in order to attempt the prognosis of AD and to extract representative features capting AD biomarkers for image classification, avoiding the necessity of expert knowledge [9, 14, 15]. The accuracy rates obtained when separating CN subjects from AD and also from MCI are quite high. Nevertheless, it is expected that performance of the prediction of the conversion of MCI patients to AD patients can be improved but this still remains a challenge.

1.1 Research Question

There are different subtypes of MCI depending on which cognitive domains are most impaired and the annual conversion rate of amnestic MCI to AD is about 12% per year [1]. However, there is not much information about other subtypes that could help in obtaining a higher accuracy prediction from MCI to AD. In addition, in almost all data collections there are no labels about the MCI subtype in MCI subjects. This is the case of the Alzheimer's Disease Neuroimaging Initiative (ADNI) database[1]. Therefore, in this project structural brain imaging data from ADNI data is used.

[1] ADNI is a longitudinal multicenter study launched in 2004 and designed to develop clinical, imaging, genetic, and biochemical biomarkers for the early detection and tracking of AD [16].

The key question addressed in this thesis is whether the conversion rate to AD is higher for any specific MCI type that could be identified based on sMRI biomarkers. This question implies the capability to find subtypes of MCI which can be clearly identified from sMRI data.
In order to address the question, the following tasks are intended:

1. To perform a relevant feature extraction and feature selection from ADNI structural MRI (sMRI) data.

2. To identify MCI subtypes from characteristics shown in data with unsupervised learning methods.

3. To study correlations between groups found in point 2 and the likelihood of progression to AD.

1.2 Aims and Scope

The aim of this project is to investigate the potential of machine learning for exploratory analysis of brain imaging biomarkers of AD in early stages. The ambition is to identify subtypes from MCI subjects. Better understanding of MRI biomarkers for detection and prediction of early stages of AD may have an important impact on successful treatments.
The amount and type of data from clinical studies is a limitation. Petersen et al. [17] suggests that approximately 16% of elderly subjects not suffering from dementia are affected by MCI, and amnestic MCI is the most common type. So one limitation is that in ADNI MCI data there will probably be more amnestic MCI subtype and it is not certain whether the four subtypes of MCI (accounting for single and multiple domain distinction) are present since MCI subtypes are not labeled in ADNI. Another limitation of using data from one study center could be to what extent an algorithm developed in one research center can be generalized to individuals examined in other centers.
Some assumptions are made in this project. First, due to time constraints, the pre-processing of image data is done in a simple way. Regions of interest (ROIs) such us the entorhinal cortex and the hippocampus volume aren't extracted by using ROI analysis extraction tools [2]. Images are cut by the edges following ICBM brain ATLAS [18]

[2]Typical neuroimaging softwares used for ROI: SPM, AFNI, FreeSurfer

in order to have a box around ROIs. This decision will reduce the performance of the exploratory study of biomarkers, which is expected to be offset by the use of state-of-the-art machine learning techniques. Another assumption is that genetic and biochemical information available in ADNI will be not used. This information could improve the results but in the project the focus is on imaging biomarkers.

1.3 Thesis outline

This thesis consists of six chapters, including the present one which serves as an introduction, and is structured as follows:

- Chapter 2, Background: Provides an overview of topics surrounding Alzheimer's Disease, enabling for a deeper understanding of the topic at hand. It also reviews the related work in the context of diagnosis and prognosis of the disease, the characterization of the different subtypes of MCI subjects, and the analysis of MRI images using machine learning.
- Chapter 3, Method: Describes all the decisions and steps done throughout this project.
- Chapter 4, Results: Contains information about the results obtained from this research.
- Chapter 5, Discussion: Analyzes the results, problems and limitations of the work.
- Chapter 6, Conclusions and Future Work: Presents the conclusions from the technical, academic, and personal point of view, and it also includes challenges and future directions.

Chapter 2

Background

2.1 Alzheimer's Disease (AD)

AD is the most common type of dementia, but there are many kinds. Dementia is characterized by the loss of cognitive functioning and behavioral abilities to such an extent that it interferes with the daily life of a person. The earliest signs are an impairment of recent memory function and attention, followed by failure of language skills, visual-spatial perception, abstract thinking and self-management. Alterations of personality inevitably accompany these defects [19].
Dementia is caused by damage to nerve cells in the brain (neurons in the brain stop working, lose connections with other brain cells and die). While everyone loses some neurons as they age, people suffering dementia experience far greater loss [20].
The majority of AD cases arise sporadically after age 60 (late-onset type of AD), but it can rarely occur between a person's 30s and mid-60s (early-onset type of AD). The most important known risk factor for AD is increasing age, about one-third of all people age 85 and older may have AD [20].
Although treatment can help manage symptoms in some people, there is currently no cure for AD. Increasing evidence that the molecular pathomechanisms of AD become active several years before neurons start dying and cognitive deficits manifests led to the concept of MCI (transitional zone between NC and AD) [1]. It is at that stage, when effective treatment would have the biggest impact since the cognitive function could be preserved.

2.2 MCI subtypes

Patients are rated based on the severity of their cognitive impairment in four domains: memory, language, visuospatial, and executive [21]. Then, it is possible to classify MCI patients in four categories defined at the first key conference on MCI [2] and based on the affected cognitive domain:

1. Amnestic MCI single domain (aMCI-s): patients with moderate to severe impairment in only the memory domain.
2. Non-amnestic MCI single domain (naMCI-s): patients with moderate to severe impairment in a non-memory single domain.
3. Amnestic MCI multiple domain (aMCI-m): patients with moderate to severe impairment in 2 or more memory domains.
4. Non-amnestic MCI multiple domain (naMCI-m): patients with moderate to severe impairment in 2 or more domains.

In Figure 2.1 the MCI classification is presented. There, it is possible to recognize that MCI could result from a variety of etiologies and not just AD.
Some studies deal with a more general classification of MCI due to limited sample size: aMCI and naMCI. While aMCI and naMCI are theoretically different entities, only a few investigations studied the structural brain differences between these subtypes of MCI.

2.3 Medical images

A medical image is the representation of the internal structure or function of an anatomic region in the form of an array of picture elements called pixels or voxels [22]. It is a discrete representation resulting from a sampling/reconstruction process that maps numerical values to positions in space.

2.3.1 Data properties

Many medical images capture volumetric images which results in large data sizes for each sample, affecting computational and memory costs

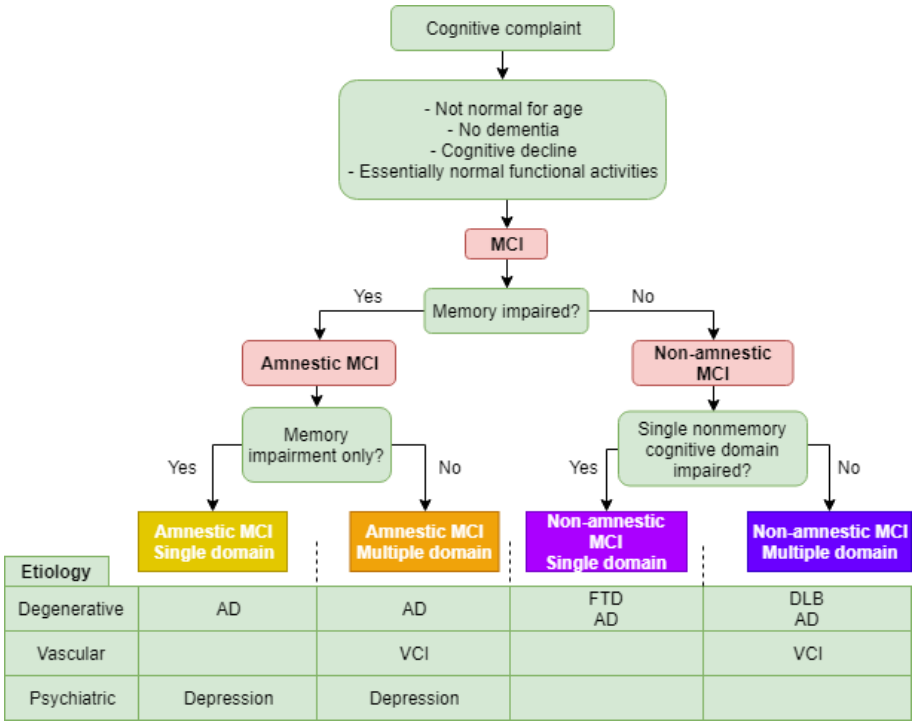

Figure 2.1: Broaden MCI classification scheme adapted from [3]. DLB = Dementia with Lewy bodies; FTD = Frontotemporal Dementia; VCI = Vascular Cognitive Impairment.

[23]. To deal with this challenge, different strategies in deep learning are used, such as working with 2D slices sampled along one axis from 3D images or the use of 3D subvolumes.
Medical images are obtained under controlled conditions allowing more predictable data distributions. However, there are some challenges, for example, the fact that small image features can have large clinical importance or that some rare pathologies can be life-threatening. To account for these challenges in medical image analysis researchers must deal with large class imbalances.

2.3.2 Data format

Medical image data is typically stored in different formats than in many computer vision tasks [23]. The image format describes how the image data is organized within the image file and how the pixel data should be interpreted by a software for the correct loading and visualization. All the information that describes the image is found in

metadata [1] and the numerical values of the pixels are found in image data [2] or pixel data.
There are two categories of medical image file formats. The first is intended to standarize the images generated by diagnostic modalities. An example from this category is DICOM (Digital Imaging and Communications in Medicine) [24]. The second is born with the aim to facilitate and strengthen post-processing analysis. Examples from this category are Analyze [25], Nifti (Neuroimaging Informatics Technology Initiative) [26] and Minc [27]. Moreover, there are two possible configurations. The most common is the one where metadata and image data are stored in the same file. However there is another configuration used by the oldest image file format that stores the metadata in one file and the image data in another one.
The characteristics of the 2 most used file formats are the following:

1. **Nifti**: Images are typically saved as a single ".nii" file with the header and image data merged. Data can be compressed which changes the file extension to "nii.gz". The file represents the 3D image of the brain. The format is supported by many viewers and image analysis software.

2. **DICOM**: DICOM standard is the backbone of every medical imaging department. It is not only a file format but also a network communication protocol. Metadata and image data are stored in a unique file (".dcm") and the header contains the most complete description of the entire procedure used to generate the image, by giving information about acquisition and also about the patient. Unlike Nifti, a Dicom file represents one slice of the brain, where a 3D volume is thus described by a series of files containing single slices. DICOM has been widely accepted and successfully used in a clinical context.

[1] Metadata is usually stored at the beginning of the file as a header and contains at least the image matrix dimensions, the spatial resolution (anatomical orientation and voxel ansiotropy), the pixel depth and the photometric interpretation [22]. It frequently contains also patient information and acquisition information.

[2] Image data is located after the header. According to the data type, pixel data is stored as integers or floating-point numbers.

2.3.3 Brain imaging techniques in AD

Brain imaging or neuroimaging techniques are a non-invasive way to visualize the structure or the activity/pharmacology of the brain. There are two main categories of neuroimaging: structural imaging and functional imaging. Structural imaging provides information about brain atrophy (loss of tissue components such as neurons, synapses, glial cells, etc), while functional imaging provides information about the human brain's function or activity [28]. The neuroimaging techniques most used in AD are the following:

- **Magnetic Resonance Imaging (MRI)**: An imaging technique that uses magnetic fields and radio waves to generate high quality 2D or 3D images of brain structures without the use of ionizing radiation (X-rays) or radioactive tracers [29]. In AD the focus is on structural MRI which is a widely used method to measure brain volumes in vivo in order to detect brain atrophy.
- **Positron Emission Tomography (PET)**: A radiotracer-based imaging technique where high radioactivity areas are associated with brain activity [30]. Typical tracers used for AD are amyloid and fluorodeoxyglucose (FDG) [28].
- **Diffusion Tensor Imaging (DTI)**: A MRI-based imaging technique sensitive to differences in the microstructural architecture of water molecules. It measures the directionality of water diffusion and makes it possible to estimate the location, orientation, and anisotropy of the brain's white matter tracts [31].

2.4 MRI biomarkers

The term biomarker or biological biomarker refers to a broad subcategory of medical signs – that is, objective indications of medical state observed from outside the patient – which can be measured accurately and reproducibly [32]. There are several definitions. The International Programme on Chemical Safety defines biomarkers as "any substance, structure, or process that can be measured in the body or its products and influence or predict the incidence of outcome or disease" [33].

Characteristics of an ideal biomarker for AD are analyzed in [34] as follows. The biomarker should:

1. Detect a fundamental feature of AD's neuropathology.
2. Be validated in neuropathologically confirmed AD cases.
3. Be precise, able to detect AD early, and distinguish it from other forms of dementias.
4. Be reliable, non-invasive, simple to perform and inexpensive.

There are three main categories of biomarkers providing additional information for AD: genetic, biochemical and neuroimaging. In this project MRI biomarkers (neuroimaging biomarkers) will be analyzed since they offer great potential as biomarkers for AD.
Atrophic changes that had been detected by structural MRI images affect primarily the entorthinal cortex and the hippocampus in an early stage of MCI, progress to temporal and parietal lobes in AD and finally involve frontal lobes in late stages of AD [1].
By using functional MRI and DTI to measure changes in functional and structural connectivity, it may be possible to detect neurons impaired by AD process but not yet irreversibly damaged (as it happens in structural imaging). These novel techniques offer new possibilities as biomarkers in AD but need standardization and validation to make them clinically useful. Thus structural MRI, in particular the hippocampus volume, remains the most validated and widely used MRI biomarker for AD [35].

2.5 Relevant unsupervised ML and visualization techniques

2.5.1 Data dimensionality reduction

Autoencoders (AEs)

An autoencoder is an artificial neural network which is trained in order to learn a representation from the original input in an unsupervised way. The network can be viewed as two parts: the encoder $\mathbf{h} = f(\mathbf{x})$ which compresses the input into a latent-space representation and the decoder that generates the reconstruction $\hat{\mathbf{x}} = g(\mathbf{h})$ from this representation. This network can be trained by minimizing the reconstruction error, $\mathcal{L}(\mathbf{x}, \hat{\mathbf{x}})$, which measures the differences between

our original input and the consequent reconstruction.
AEs have typically been used for dimensionality reduction or feature learning. Recently, they have been more widely used for generative models of data [36]. Autoencoders may be thought of as being a special case of feedforward networks, and may be trained with the same techniques, typically minibatch gradient descent following gradients computed by back-propagation. If the autoencoder is built as a linear network, then the optimal solution is strongly related to the dimensionality reduction in principal component analysis (PCA).

- **Convolutional autoencoder**

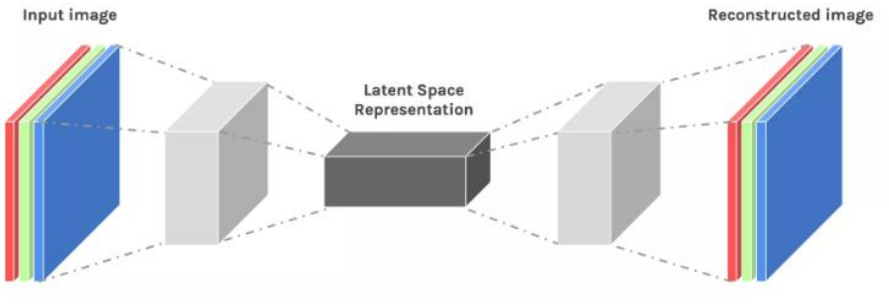

Figure 2.2: Structure of a convolutional autoencoder.

A common use for autoencoders is to apply them to image data. When dealing with images the standard procedure is to replace fully connected layers by convolutional layers.
By using convolutional and pooling layers the encoder converts the input from wide and thin to narrow and thick. This helps the network to extract visual features from the images, and therefore obtains a much more accurate latent space representation. In each convolutional layer a set of filters (also called kernels) are applied to the input layer, which consists of a 3D tensor (width, height and number of channels). The outputs of the convolutions with the different filters are stacked and form a new image. Then, a non-linear activation function is applied to each element of this new image, typically the rectified linear unit (ReLU) activation. ReLU performs the easy operation of $\mathbf{h} = max(0, \mathbf{x})$. Finally, sometimes a pooling layer is applied to reduce the spatial size of the representation and thus reduce the number of network parameters. It operates over each response/activation map independently. The most common approach used is max pooling,

which applies a window function to the input patch, and computes the maximum in the neighborhood.
The decoder uses upsampling and convolutional layers to reconstruct the data. The upsampling layer upsamples the input image to a higher resolution by using resampling and interpolation.

PCA

Principal Components Analysis (PCA) is an unsupervised approach where a set of linearly uncorrelated variables (eigenvectors) and their corresponding values (eigenvalues) are computed by using an orthogonal transformation (Singular Value Decomposition). It aims to find a lower-dimensional subspace onto which to project the data. The dimensions with large eigenvalues are chosen since they contain lots of variation and are therefore useful dimensions, while the ones that have small eigenvalues are discarded since there is not much variation in that direction [37].
The common applications are dimensionality reduction in order to significantly speed up our feature learning algorithm and data visualization. PCA is sensitive to the relative scaling of the original variables.

t-Distributed Stochastic Neighbor Embedding

t-Distributed Stochastic Neighbor Embedding (t-SNE) is a dimensionality reduction technique particularly well suited for the visualization of high-dimensional data. [38].
t-SNE converts similarities between data points to probability distributions and tries to minimize the Kullback-Leibler divergence between the probability distributions of the low-dimensional embedding and the high-dimensional data. Its cost function is not convex, which means that with different initializations different results can be obtained.
There are two characteristic parameters in t-SNE: perplexity (related to the number of close neighbors each point has) and early exaggeration (related to how tight natural clusters in the original space are in the embedded space and how much space will be between them).

2.5.2 Clustering

The two most relevant clustering techniques for this project are explained below:

- **Density-Based Spatial Clustering of Applications with Noise (DBSCAN)**
  DBSCAN is a density based clustering technique that creates an arbitrary number of clusters in areas with high density, and assumes they are separated by areas of lower density. One of the main advantages is that it does not require the number of clusters in the data to be specified a priori. Another advantage is that it has a notion of noise. It is governed by the two parameters *eps* and *min_samples* which have to be found by exhaustive search.
  eps is the maximum distance between two samples for them to be considered as being in the same neighborhood and *min_samples* is the minimum number of samples in a neighborhood required to form a dense region.
  DBSCAN can be seen as an efficient variant of spectral clustering where the connected components found correspond to optimal spectral clusters.

- **Agglomerative Clustering**
  Agglomerative Clustering attempts to cluster the data hierarchically, using a bottom up approach. The algorithm starts with each point in its own cluster and then, for each cluster, uses some criterion to choose another cluster to merge with [39]. The algorithm merges by using a linkage metric, the default being Euclidean. The clusters are linked together if they minimize this distance.

2.5.3 Manifold visualization

In order to visualize the structure of a high-dimensional dataset, its dimension must be reduced. One approach is to assume that the data lies on an embedded non-linear manifold within the high-dimensional space. Then, the data can be visualized in the low-dimensional space of the manifold. A widely used technique to perform manifold visualization is t-SNE, introduced in subsection 2.5.1. Figure 2.3 shows the manifold visualization done in [15] of AD, CN and MCI subjects. This visualization is performed after each convolution step from the pretrained 3D CAE and it shows that data is more separable each time.

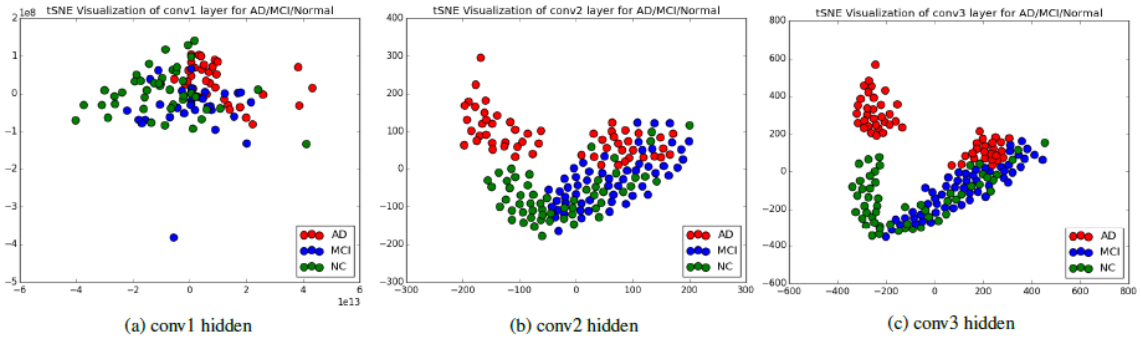

(a) conv1 hidden (b) conv2 hidden (c) conv3 hidden

Figure 2.3: Manifold visualization of ADNI training data, by t-SNE projection adapted from [15].

2.6 Related Work

2.6.1 ML for identification of MRI biomarkers of AD

In later years, machine learning techniques started to be applied in order to have better diagnosis and prognosis of AD. Haller et al. [4] obtained a highly accurate individual classification of stable versus progressive MCI regardless the MCI subtype. They performed a SVM analysis of 35 NC and 67 MCI subjects with DTI baseline data recruited in Geneva and Lausanne counties. Nho et al. [5], who also used SVM with radial basis function kernels, predicted the conversion of amnestic MCI to AD using ADNI data. They discarded the other subtypes as it is shown that the amnestic subtype is the most considered subtype of the prodromal phase of AD. They obtained 90.5% cross-validation accuracy for classifying AD and NC, and 72.3% accuracy for predicting MCI conversion to AD. Features were extracted using two analysis techniques, one using FreeSurfer software (a brain segmentation and cortical parcellation tool) and the other using SPM5 (Statistical Parametric Mapping tool). The best prediction of MCI conversion to probable AD was obtained for a number of features between 24 and 26. The most important feature identified was left entorhinal cortical thickness. The other two were right hippocampal volume and APOE $\epsilon 4$ status.

One year later Costafreda et al. [6] used just the hippocampal volume to predict MCI subjects that will convert to AD. The study consists of 103 MCI subjects from the AddNeuroMed study. Preprocessing of

data is performed by FreeSurfer and the classification analysis consists of a SVM with non-linear Gaussian radial basis kernel. The model was trained on the full training sample of AD and NC subjects and then applied to MCI subjects. The accuracies achieved within a year are 85% for AD vs NC and 80% for the MCI conversion to AD. Finally they stated that the incorporation of entorhinal atrophy could increase the prognostic performance relative to the analysis of hippocampal changes alone.

SVM is one of the most used techniques when classifying AD versus CN and sMCI versus pMCI; in [10] a critical review of different SVM studies is provided. These used both structural and functional neuroimaging, applied in the context of disease diagnosis, transition prediction and treatment prognosis.

In 2015, five key features that potentially discriminate between MCI subjects who convert to AD and stable MCI patients over a period of three years were provided in Eskildsen et al. [7]. These features are the left and right hippocampus, cortical thicknesses of left precuneus, left superior temporal sulcus, right anterior part of the parahippocampal. They achieved an accuracy of 72% using ADNI data.

With the growing availability of data for AD and CN subjects, Ning et al. [13] used brain imaging and genetic data from ADNI (138 AD patients, 225 CN subjects and 358 MCI patients) for these AD classification and prediction tasks. They trained a neural network (NN) and Logistic Regression (LR) to classify AD versus CN subjects given brain and genetic features as predictors. The most important brain features found in the NN model were the left middle temporal gyrus, the left hippocampus, the right entorhinal cortex volume, the left interior lateral ventricle and the right inferior parietal lobe. And the most relevant genetic feature was APOE $\epsilon 4$ risk allele.

In March of 2018 Liu et al. [9] stood out with the proposed Cascaded Convolutional Neural Network (CNN) that can gradually and automatically learn the multi-level and multimodal features of MRI and PET brain images for AD classification. Since no image segmentation and rigid registration are required in pre-processing data, an expert's knowledge is not necessary, which is an advantage with respect to other studies where they extract hand-craft imaging features and then train a classifier. The study consists of 93 AD patients, 204 MCI patients and 100 NC subjects from ADNI. The accuracies achieved are 93.26% for classification of AD vs NC and 82.95% for classification of

progressive MCI vs NC.
Also in 2018, Duraisamy et al. [8] developed a classification algorithm which combines both supervised and unsupervised learning techniques and analyzed the brain images from ADNI related to sMRI for better discrimination of AD, CN and MCI labels. ROIs related to Hippocampus and Posterior Cingulate Cortex from the brain images are extracted using an Automated Anatomical Labeling (AAL) method at the first stage. Then 19 highly relevant AD related features are selected through Multiple-criterion feature selection method. Finally, they apply their novel FCM-based Weighted Probabilistic Neural Network (FWPNN) classification algorithm. The accuracies achieved are 98.63% for AD vs NC, 95.4% for MCI vs NC and 96.4% for AD vs MCI.

2.6.2 Analysis of MCI subtypes

In 2006 Yaffe et al. [21] studied different subtypes of MCI and assessed the rate of progression to dementia. They found that there is a correlation between the conversion to different types of dementia and prior subtypes of MCI. In addition, among the patients who evolved to AD, 76% had amnestic MCI, 11% single non-memory MCI and 16% multiple domain MCI. This explains why many studies focus on the amnestic subtype of MCI.
One year later, a comparison of the rates of conversion to AD between 2 subtypes of MCI is done by Fischer et al. [40]. The study was done with 141 MCI patients at age 75 and followed up after 30 months which were categorized into 2 subtypes: amnestic and non-amnestic. Conversion rates to AD were 48,7% for amnestic, 26.8% for non-amnestic, while for NC it was 12,6%. Although the rate of conversion was higher for amnestic MCI than for non-amnestic MCI, nearly identical numbers of subjects developed AD from each subtype. Therefore two categories were not useful in identifying early stages of various types of dementia.
A differentiation between amnestic and non-amnestic MCI by structural MRI is done in Csukly et al. [41]. 62 subjects with aMCI, naMCI and NC were included in the study based on the Petersen criteria [2]. They were recollected in the Department of Psychiatry and Psychotherapy, Semmelweis University, Budapest. The volumes of the hippocampus and the entorhinal cortex, and the thickness of the entorhinal cortex and the fusiform gyrus are significantly decreased in

the aMCI relative to the naMCI group. But the largest difference was detected in the volume and thickness of entorhinal cortex, which is in line with the fact that the atrophy in AD starts in this region. Based on their results MRI can be a useful tool for the more precise separation of MCI subtypes. They conclude that the assignment of MCI subtypes will be useful to improve the prediction of dementia type and the risk of conversion to dementia.

2.6.3 Exploratory analysis of MRI images using ML

An MRI scan usually contains hundreds of millions of voxels (volume elements that represents a value in the 3D space, corresponding to a pixel for a given slice thickness). The amount of noise voxels is much larger than the informative voxels and makes typical machine learning algorithms, such as SVM, have a lower performance. Moreover this represents a high computational cost.
When working with SVM classifiers it is necessary to suppress non informative voxels from MRI scans and reduce its dimensionality. One option is the use of voxels in a particular ROI instead of using the whole brain. There are many available tools that allow ROI extraction and other processing operations such as FSL [42], FreeSurfer [43] and SPM [44]. This feature extraction process normally needs expertise knowledge about the underlying problem.
Meaningful features were designed mostly by human experts on basis of their knowledge about the target domain, making it challenging for nonexperts to exploit machine learning techniques for their own studies [45]. However, recently, thanks to the success of deep learning methods, feature extraction process requires no longer expert's knowledge. Deep learning is able to discover the discriminant representations inherent in data by incorporating the feature extraction into the task learning process. Complex patterns can be learned with deep learning.
CNNs have been explored to learn generic features of neuroimages for AD and other purposes. In 2015 Payan et al. [14] proposed a sparse autoencoder (AE) and 3D convolutional neural networks based on both structural and functional MRI data to predict the AD status of a patient. The difference of this approach compared to other classifiers is that the whole MRI image is used, which yields better performance than using slices from the brain and 2D CNNs. Randomly selected

3D patches of size 5x5x5 extracted from MRI scans are used to train the sparse AE. Later, the trained weights from the autoencoder are used as 3D convolutional filters of 3D CNN. Finally, the fully connected layers of 3D CNN are fine-tuned for classification (the convolutional layer is pre-trained but not fine-tuned). One year later Hosseini et al. [15] proposed a deep 3D CNNs method to predict AD using structural MRI scans from ADNI. The 3D CNNs was built, similar than in [14], upon 3D Convolutional AEs pre-trained on CADDementia dataset, followed by fully connected network for classification. Although both methods used in [14, 15] can learn generic features capturing AD biomarkers, they require the convolutional filters pre-trained on AE with carefully preprocessed data.
There are more works where deep learning has been successfully applied to MRI data. In 2013 Shin et al. [46] used stacked AEs (SAEs) to detect multiple organs in a time series of 3D MRI data by separately learning both visual and temporal features from an unlabeled multimodal DCE-MRI dataset. Unlike conventional SAEs, the SAE in this study involved the application of a pooling operation after each layer so that features of progressively larger input regions were essentially compressed. They showed the potential of the deep learning model for application to medical images, despite the difficulty of obtaining libraries of correctly labeled training datasets and despite the intrinsic abnormalities present in patient datasets.

Deep learning has been also explored for segmentation tasks, such as the important step in the brain image preprocessing which is removing nonbrain regions such as the skull. Kleesiek et al. [47] presented a 3D convolutional deep learning architecture for brain extraction in 2016, a technique that was not limited to nonenhanced T1-weighted MR images (it is applicable to MRI data including 4 channels). While training their 3D CNN, they constructed minibatches of multiple cubes that were larger than the actual input to their 3D CNN for computational efficiency. Over three different data sets, their method achieved the highest average specificity measures in comparison to six commonly used tools (BET, BEaST, BSE, ROBEX, HWA, and 3dSkullStrip), whereas its sensitivity displayed about average results. Another segmentation task difficult to perform is segmentation of infants' brain MR images. Comparing to adults' brain, in infants' brain tissue contrast is reduced, noise is increased and, WM and GM exhibit similar

levels of intensity [45]. In 2015 Zhang et al. [48] proposed 4 CNN architectures to segment isointense stage (infants of approximately 6-8 months age) brain tissues using multimodal MRI scans. To each CNN 3 convolutional layers, one fully connected layer and an output layer with a softmax operation for tissue classification are applied. Each CNN included three input feature maps corresponding to T1, T2 and fractional ansiotropy (FA) images patches measuring 13x13 voxels. Results showed that the proposed model significantly outperformed competing methods on infant brain tissue segmentation. In 2016 Pereira et al. [49] presented an automatic segmentation method based on CNNs. They explored small-sized 3x3 kernels, the use of intensity normalization as a preprocessing step (not common in CNN-based segmentation methods) and data augmentation which proved to be very effective for brain tumor segmentation in MRI data. They trained different CNN architectures for low and high grade tumors. Their method was validated in the 2013 Brain Tumor Segmentation (BRATS) Challenge, where they obtained the first position for the complete, core, and enhancing regions for the Challenge dataset.

Chapter 3

Methods

The work of this project is structured as in Figure 3.1 and the code can be found in my KTH and my personal git repository [1].

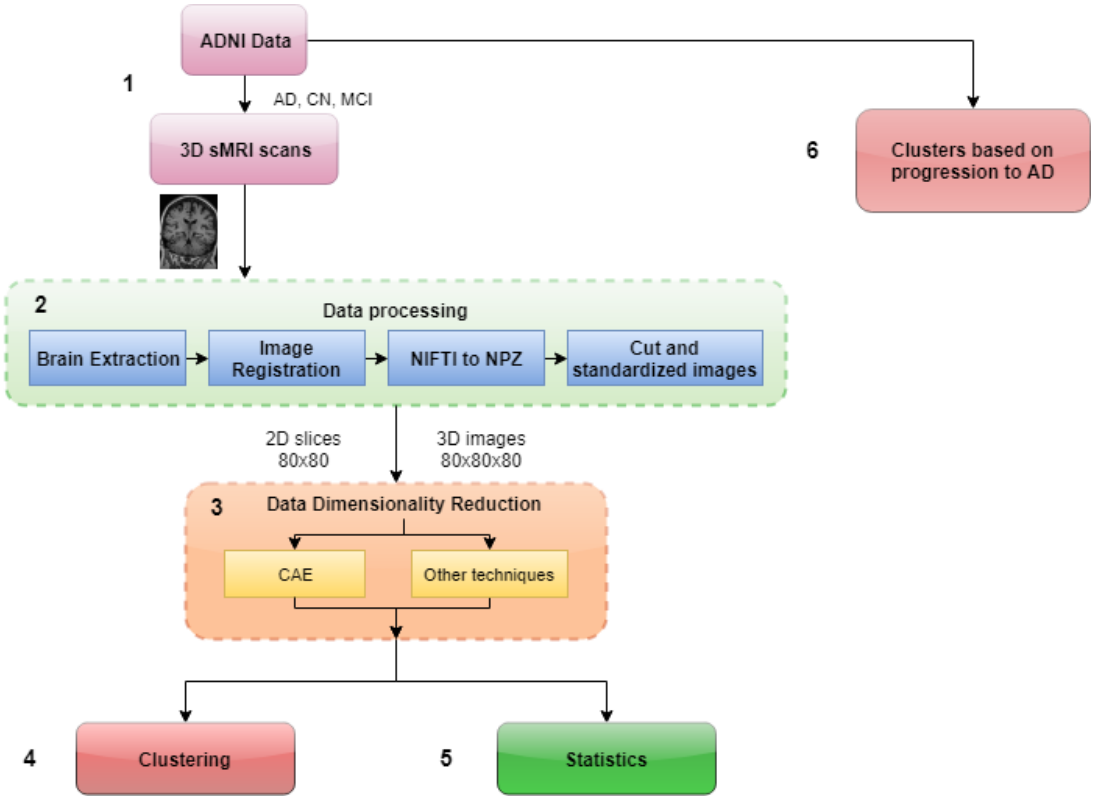

Figure 3.1: Diagram of all the steps of the study process.

[1] KTH git repository: https://gits-15.sys.kth.se/annacg/Master-thesis
Personal git repository: https://github.com/annacanal/Master-thesis

The steps done in this project are highlighted in Figure 3.1, where each number corresponds to the respective step. The first step (1) is the decision, selection and acquisition of the data to be used in the study. Structural MRI scans of AD, MCI and CN subjects from ADNI Data Collection are downloaded. Structural MRI is chosen as the neuroimaging technique since it is the most common approach in previous related work. Similarly, ADNI database is chosen because, to the best of my knowledge, it is the largest AD database and the most used in previous work. This step is detailed in Section 3.1.
The second step (2) is to prepare the data for the application of machine learning techniques. Four different standard processing steps are performed according to the standard pre-processing done in previous studies in which domain-specific MRI pre-preprocessing is not performed either [9]. These pre-processing steps will be explained in Section 3.2
The third step (3) is to reduce the dimensionality of the data. Several techniques are used, but the main focus has been on the development of a CAE model which was motivated by the work in [15]. CAE's structure and parameters, and the configuration of other techniques such as PCA and tSNE are described in Subsection 3.3 for the application of dimensionality reduction.
Once the dimensionality of the images is reduced two clustering techniques (4) are applied and a study of similarities of the data within groups and dissimilarities of the data between different groups is performed (5).
Finally, by using the follow-up information, six clusters of MCI patients are generated regarding its progression to AD (6). This is explained in Section 3.6.

3.1 Data

A total of 1069 sMRI scans of CN, MCI and AD patients with several years of follow-up data from ADNI[2] database are selected for this project. There are 3 different phases of ADNI to date: ADNI1, ADNI GO/2 and ADNI3. In this project the images are from a standardized

[2]The database is publicly available in http://adni.loni.usc.edu. ADNI participants consist of AD, MCI and elderly CN, aged 55-90 years and recruited across North America during each phase of the study.

set with 1.5T MRI scans collected during ADNI1[3] phase, which consists of 522 MCI scans, 243 AD scans and 304 CN scans. There are 2 scans for almost all the subjects.

3.1.1 ADNI1 Standardized Data Collections

Standardized Data Collections are collections of pre-processed scans corresponding to each of the standardized datasets created in order to speed up the download of images for researchers. The file format used in these collections is Nifti.
Collection names and descriptions from ADNI1 for 1.5T scans are shown in Table 3.1.

Table 3.1: ADNI1 Standardized Data Collections for 1.5T [50].

Collection Name	Collection Description
ADNI1: Screening 1.5T	Contains screening or baseline scans
ADNI1: Complete 1Yr 1.5T	Contains screening, 6 and 12 months scans
ADNI1: Complete 2Yr 1.5T	Contains screening, 6 months, 1 year, 18 months (MCI only) and 2 year scans
ADNI1: Annual 2 Yr 1.5T	Contains screening, 1, and 2 years scans
ADNI1: Complete 3Yr 1.5T	Contains screening, 6 months, 1 year, 18 months (MCI only), 2 years, and 3 years (normal and MCI only) scans

ADNI1: Screening 1.5T is the standardized data collection downloaded for this project in order to have as much data as possible to train and test. Follow-up scans are not necessary since the study is based on differences between groups of patients, in concrete within MCI subjects, during the baseline. What is needed is the follow-up information about the evolution of MCI patients and this is provided by an Excel document. Patients with follow-up data are needed but the analysis is performed during the baseline.

[3]ADNI1(2004-2009) contains in total 200 CN subjects, 400 MCI subjects and 200 mild AD subjects. The MRI protocol used in ADNI1 focuses on consistent longitudinal structural imaging on 1.5T scanners using T1- and dual echo T2-weighted sequences. One-fourth of ADNI1 subjects were also scanned using essentially the same protocol on 3T scanners.

3.1.2 MRI scans

In order to visualize the MRI scans saved in the Nifti format, FSL software is used. Figure 3.2 shows the visualization of an AD patient using FSL eyes tool.

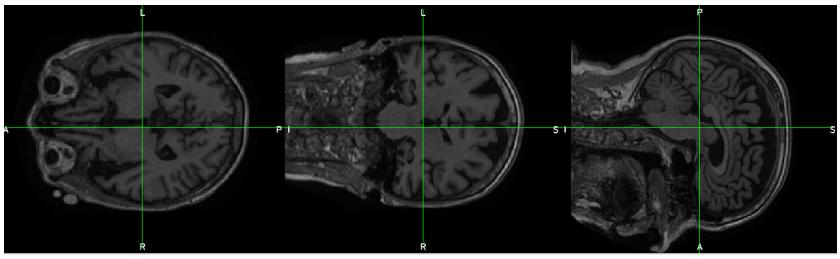

Figure 3.2: MRI scan of an AD patient.

3.2 Data processing

3.2.1 Brain extraction tool (BET)

FSL is used in order to process the data. FSL is a comprehensive library of analysis tools for fMRI, MRI and DTI brain imaging data [42]. The tool used in this project to extract brain tissue from images is the Brain extraction tool (BET). BET is an automated method for segmenting magnetic resonance head images into brain and non-brain by deleting the non-brain tissue from them [51], which is a crucial step in many analysis pipelines.

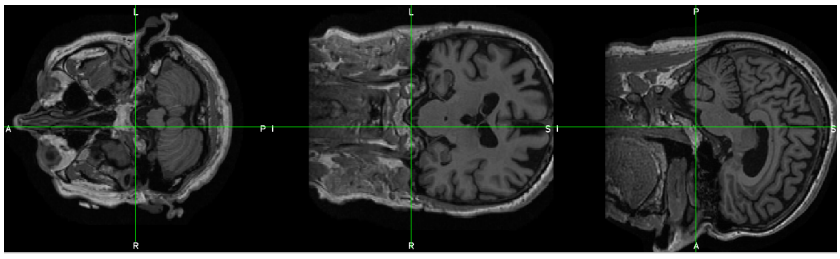

Figure 3.3: MRI scan of a MCI patient before applying BET.

A script is made to generate all the commands needed to apply BET the data using its default parameters. Figure 3.4 shows a MRI scan before and after applying BET. The Brain extraction tool method does

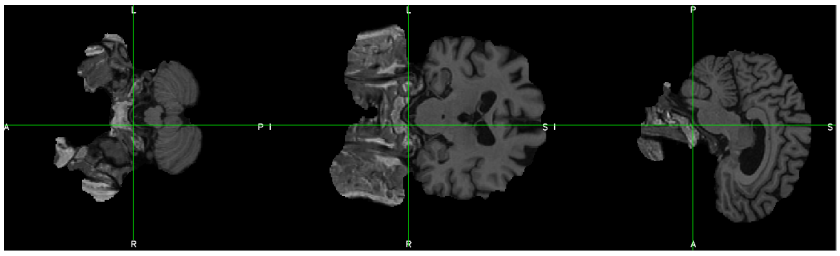

Figure 3.4: MRI scan of a MCI patient after applying BET.

not require any pre-processing before application, and it does not take much time to process data.

3.2.2 Conversion of Nifti data to compressed numpy arrays

The NiBabel [52] module is used in order to access data in neuroimaging file formats. It is used to load the MRI scans and get the image data from Nifti images. Nibabel is a pure Python package which can be installed using pip. A NiBabel image contains:

- The image data array: a 3D or 4D array of image data. Figure 3.5 shows the image data of one MRI scan.
- An affine array: gives information about the position of the image array data in a reference space. Figure 3.6 shows the affine array from one MRI scan.
- Image metadata: In form of an image header, it describes the image. The header is shown in Figure 3.7.

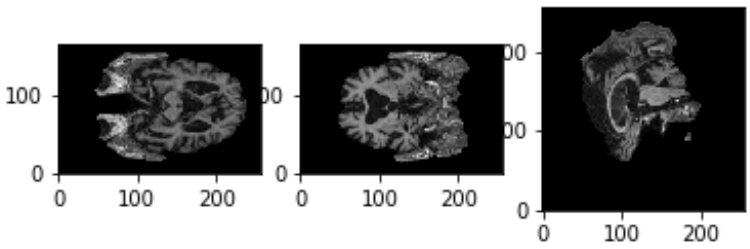

Figure 3.5: Center slices of a MRI scan from an AD patient.

```
print(img256.affine)
```

```
[[ 0.00000000e+00 -3.91699517e-09 -1.20370150e+00  1.00268997e+02]
 [-3.94953403e-09 -1.01561999e+00  4.64237937e-09  1.45979996e+02]
 [-1.02405679e+00  3.91699517e-09  0.00000000e+00  1.25054001e+02]
 [ 0.00000000e+00  0.00000000e+00  0.00000000e+00  1.00000000e+00]]
```

Figure 3.6: Affine array information.

```
<class 'nibabel.nifti1.Nifti1Header'> object, endian='<'
sizeof_hdr      : 348
data_type       : b''
db_name         : b''
extents         : 0
session_error   : 0
regular         : b'r'
dim_info        : 0
dim             : [  3 256 256 166   1   1   1   1]
intent_p1       : 0.0
intent_p2       : 0.0
intent_p3       : 0.0
intent_code     : none
datatype        : float32
bitpix          : 32
slice_start     : 0
pixdim          : [1.        1.0240568 1.01562   1.2037015 1.        0.        0.
 0.       ]
vox_offset      : 0.0
scl_slope       : nan
scl_inter       : nan
slice_end       : 0
slice_code      : unknown
xyzt_units      : 10
cal_max         : 0.0
cal_min         : 0.0
slice_duration  : 0.0
toffset         : 0.0
glmax           : 0
glmin           : 0
descrip         : b'5.0.11'
aux_file        : b'none'
qform_code      : scanner
sform_code      : scanner
quatern_b       : 0.70710677
quatern_c       : -2.7271363e-09
quatern_d       : -0.70710677
qoffset_x       : 100.269
qoffset_y       : 145.98
qoffset_z       : 125.054
srow_x          : [ 0.0000000e+00 -3.9169952e-09 -1.2037015e+00  1.0026900e+02]
srow_y          : [-3.9495340e-09 -1.0156200e+00  4.6423794e-09  1.4598000e+02]
srow_z          : [-1.0240568e+00  3.9169952e-09  0.0000000e+00  1.2505400e+02]
intent_name     : b''
magic           : b'n+1'
```

Figure 3.7: Header information of a MRI scan.

Finally the image data array is saved in a numpy array and compressed which results in a ".npz" file format.

3.2.3 Normalization

Image registration or Spatial Normalization

Since human brains differ in size and shape the use of spatial normalization is necessary. The aim of this normalization is the spatial transformation of brain scans into a common space, making them comparable to each other [53]. This is also known as image registration, which is the process of transforming different sets of data into one coordinate

system.
There are two commonly used neuroimaging reference spaces: Talairach and MNI (proposed by Montreal Neurological Institute). By using Nilearn, a neuroimaging package from Sklearn [54], data is resampled to an MNI space. A 3-dimensional nonrigid transformation model for warping a brain scan to the ICBM152 template (the current standard MNI template) is used. Linear ICBM Average Brain (ICBM152) Stereotaxic Registration Model is an average of 152 T1-weighted MRI scans, linearly transformed into the common MNI152 coordinate system, which is based on Talairach space. This template is widely used, for example in FSL and in SPM. Figure 3.8 shows the same scan from Figure 3.5 after transforming it to the ICBM152 template.

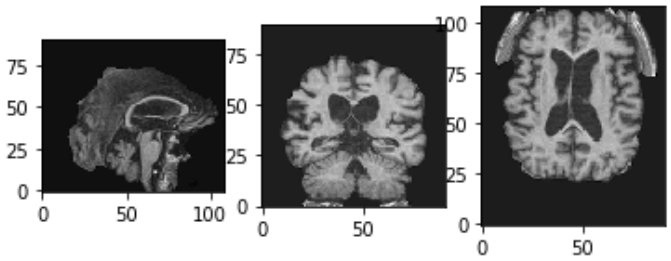

Figure 3.8: Center slices of a resampled MRI scan from an AD patient.

```
Shape comparison:
- Original image shape: (256, 256, 166)
- Resampled image shape: (91, 109, 91)
- Template image shape: (91, 109, 91)

Affine comparison:
- Original image affine:
 [[ 0.00000000e+00 -3.91699517e-09 -1.20370150e+00  1.00268997e+02]
 [-3.94953403e-09 -1.01561999e+00  4.64237937e-09  1.45979996e+02]
 [-1.02405679e+00  3.91699517e-09  0.00000000e+00  1.25054001e+02]
 [ 0.00000000e+00  0.00000000e+00  0.00000000e+00  1.00000000e+00]]
- Resampled image affine:
 [[  -2.    0.    0.   90.]
 [   0.    2.    0. -126.]
 [   0.    0.    2.  -72.]
 [   0.    0.    0.    1.]]
- Template image affine:
 [[  -2.    0.    0.   90.]
 [   0.    2.    0. -126.]
 [   0.    0.    2.  -72.]
 [   0.    0.    0.    1.]]
```

Figure 3.9: Affine array and shape information of the original image, the resampled image, and the template.

In Figure 3.9 one can observe how the image size and its affine matrix change to the same as the template. Independently of the original images size and orientation, after applying the transformation to the MNI152 space all of them are comparable. All the image data has the dimension 91x109x91.

Cut images

After the spatial normalization, data is cut to dimension 80x80x80 in order to have a zoom in the ROI. Figure 3.10 shows a scan after this zoom.

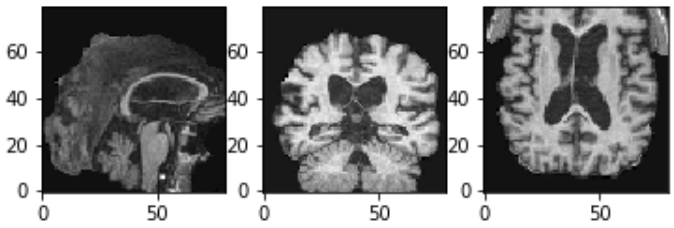

Figure 3.10: Edges of the 3D image array from an AD patient are cut to dimension 80x80x80.

Standardization

Finally, data is centered to the mean and component wise scaled to unit variance, which is a common pre-processing in machine learning, by using sklearn.preprocessing package. Figure 3.11 shows a scan after this procedure.

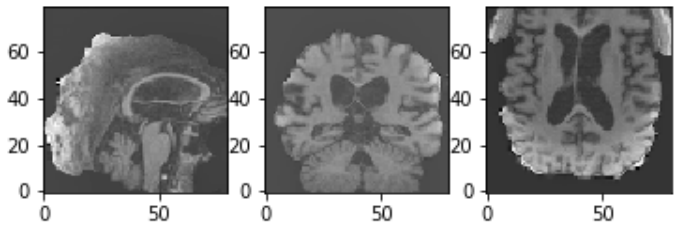

Figure 3.11: Center slices of a resampled and standarized MRI scan from an AD patient.

2D Slices

2D slices over the first, second, and third dimensions of the 3D numpy array are used in order to compare the performance of using 3D or 2D data.

3.3 Data dimensionality reduction

3.3.1 CAE

Figure 3.12 shows the structure of the CAE developed in this project when the input are 3D images.

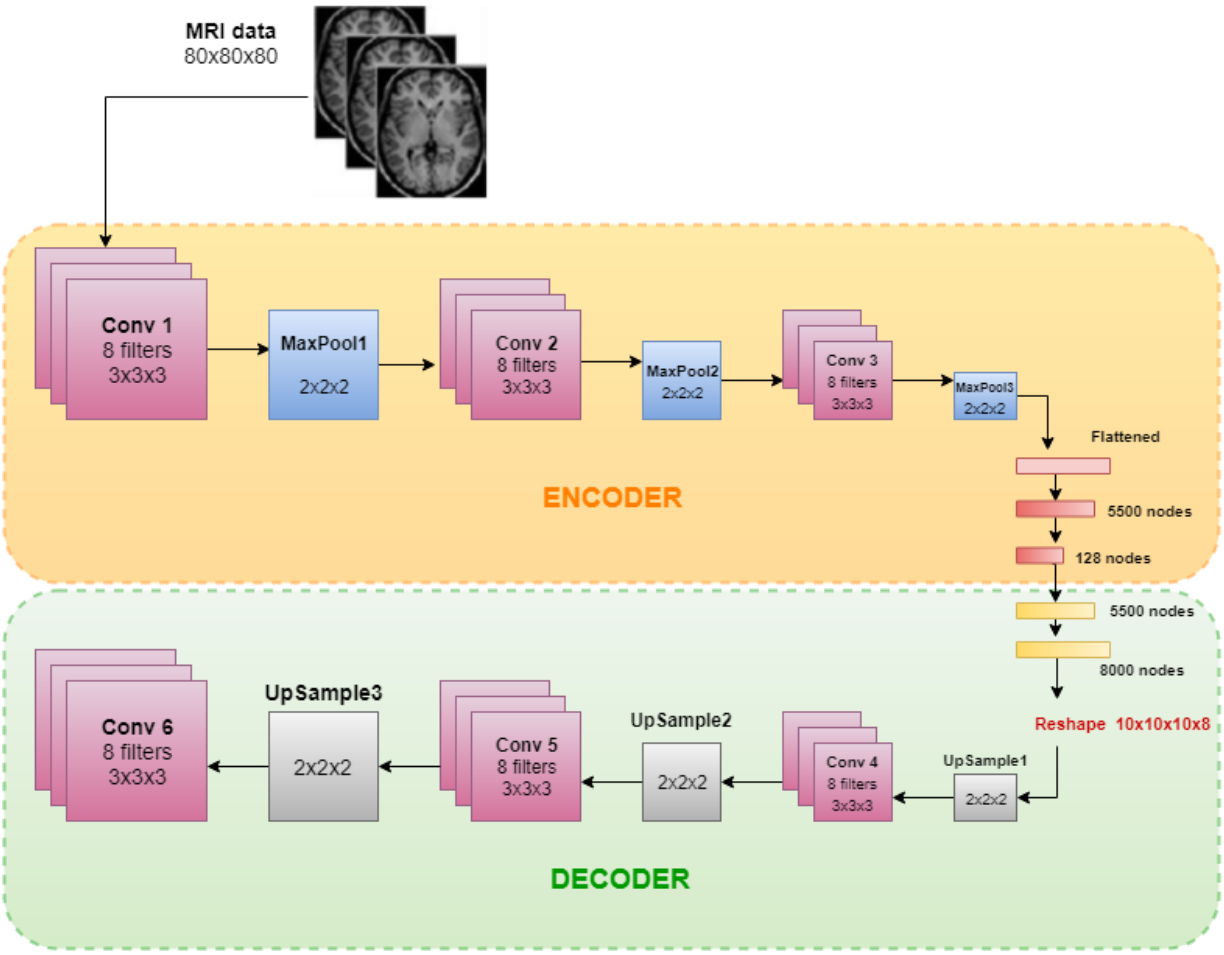

Figure 3.12: CAE structure for 3D data input.

The encoder consists of three convolutional layers with 8 filters of dimension 3x3x3, three max-pooling layers with filters 2x2x2, a fully connected layer and two dense layers with 5500 nodes and 128 nodes respectively. The fully connected layer produces a feature vector of dimension 8000. The decoder consists of two dense layers with 5500 nodes and 8000 nodes, with the final layer to be able to reshape data into dimension 10x10x10x8, followed by the same convolutional layers as in the encoder and three upsampling layers with the same filters as in max-pooling layers. The commonly used rectified linear unit (RLU) is selected as the activation function.
The CAE is trained with 60% of the data, while the remaining 40% is for testing. The loss function is the cross entropy loss and the optimization is done by using the Adadelta algorithm with a learning rate of 0.1 (which is reduced by a factor of 2-10 when the validation loss has stopped improving). The model training is stopped when the validation loss has stopped improving (with patience bigger than for the learning rate decay). The CAE is trained in PDC [4] which is a High Performance Computing center at KTH, Royal Institute of Technology [56]. The data is stored in CFS[5] system since it occupies a large amount of memory. CAE is executed on TEGNER compute nodes and uses K80 GPUs.
The implementation of this CAE has been done with Keras library [57] (open source neural network library written in Python) running on top of TensorFlow [58] (open-source software library). This architecture presented in Figure 3.12 has the same number of convolutional layers with the same characteristics (size and number of filters) as the CAE used in [15], with the addition of the dense layers to force a smaller compressed representation of the images.
A dimensionality reduction analysis with 2D slices from MRI scans is performed with the same CAE structure but then there are 2D filters and the first dense layer in the encoder has 512 nodes, instead of 5500.

[4]It is the largest and fastest high performance computing (HPC) system in Sweden. The main HPC system at PDC is Beskow. PDC's services are made available to Swedish and European researchers, via the Swedish National Infrastructure for Computing (SNIC) and PRACE respectively. SNIC is a national research infrastructure that provides a balanced and cost-efficient set of resources and user support for large scale computation and data storage to meet the needs of researchers from all scientific disciplines and from all over Sweden [55].

[5]CFS system or Lustre is one of the two storages systems of PDC. It is a parallel file system highly optimized for fast access with computational processes.

3.3.2 PCA

A linear dimensionality reduction is done by using PCA function from Scikit-learn library in order to compare with the reduction from CAE. To use this function, data is first standardized to have zero mean and unit variance. The parameters used are the default, except for the dimensions. Data is reduced to 128, 50 and 2 dimensions.

3.3.3 t-SNE

t-SNE is used to reduce the dimensionality of the data to 2 dimensions and compare the performance with the other dimensionality reduction techniques. The parameters are the default except for *perplexity*, *early exaggeration* and *learning rate*. *Perplexity* is fixed to a value of 20 while different *early exaggeration* values (12, 50 and 80) and *learning rate* values (500 and 650) are evaluated.
Moreover, it is also used to visualize the data reduced in 2D by the CAE. Scikit-learn [54] library is used for the implementations of t-SNE in both dimensionality reduction and visualization applications.

3.4 Clustering

Kmeans was used as the first clustering technique since it is an easy and well known algorithm. Then exploration of agglomerative and DBSCAN clustering is performed by using Scikit-learn [54] library. In agglomerative clustering, the Euclidean distance is used together with ward linkage which minimizes the variance of the clusters being merged. In DBSCAN the euclidean distance is used as a metric and different *eps* values and *min_samples* values are evaluated.

3.5 Data statistics

A statistical analysis of the processed 3D MRI scans and the reduced data (by the CAE, PCA and t-SNE) is done in order to check the similarities and differences within groups and between groups of patients. The purpose of a similarity measure is to give a value indicating how well two samples match. Motivated by the work in [59] where an evaluation of eight different similarity measures for MRI images is done,

Pearson correlation[6] is chosen as a similarity measure. The Pearson product-moment correlation coefficient r_{xy} for two samples is calculated as follows:

$$r_{xy} = \frac{\sum_{i=1}^{n}(x_i - \bar{x})(y_i - \bar{y}))}{\sigma_x \sigma_y} \tag{3.1}$$

where n is the sample size, $\bar{x}$ and $\bar{y}$ the sample means ($\bar{x} = \frac{1}{n}\sum_{i=1}^{n} x_i$), and σ_x and σ_y are the standard variations of the each sample ($\sqrt{\sum_{i-1}^{n}(x_i - \bar{x})^2}$).

Pair-wise Pearson correlation is calculated for all the images of each group of patients and then between images from different groups. The studied groups are first AD, CN and MCI; and later subgroups of MCI (explained in Section 3.6). In this project Pearson correlation implementation from scipy library is used.

3.6 Clusters based on progression to AD

MCI patients from ADNI with follow-up until 5-10 years are clustered into different groups with respect to their progression to AD (if they develop AD or not, and if they do, after how many years from the baseline). These groups are the following:

1. Stable MCI: patients that remain stable during all the follow-up years.
2. Progressive 1: Patients which progress to AD within a year.
3. Progressive 2: Patients that progress to AD in 2 years.
4. Progressive 3: Patients that progress to AD in 3 years.
5. Progressive 4: Patients that progress to AD in between 3 and 5 years.
6. Progressive 5: Patients that progress to AD in more than 5 years.

[6] Pearson correlation is the most widely-used type of correlation and it is also called linear or product-moment correlation. It is a measure of the linear correlation between two random variables X and Y and takes values between +1 and -1.

Chapter 4

Results

4.1 Analysis of different groups of patients with the reduced data

First of all, from the CAE's structure explained on 3.3, four different models are built and trained with pre-processed MRI images from AD, CN and MCI patients. The first model is trained with 3D scans and the other three with 2D slices over each dimension. In those four models, all the groups of patients are used since the data is labeled, which makes it possible to test if the CAE as the dimensionality reduction and feature extraction approach is helpful to cluster the data. Furthermore, it helps to decide whether latent representations obtained with the CAE are more suitable for further analysis with 3D scans or 2D slides.

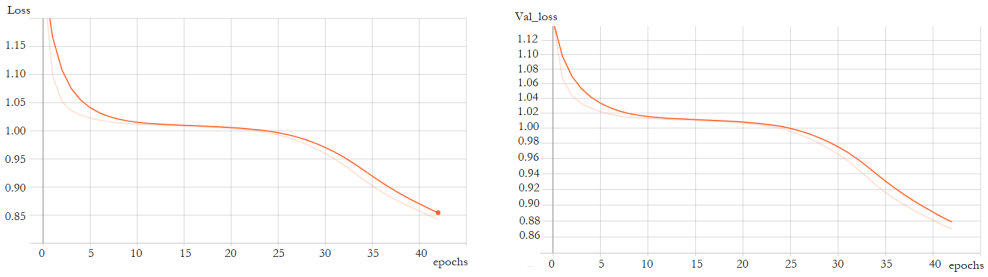

(a) Training loss

(b) Validation loss

Figure 4.1: Training and validation loss functions of CAE with input images of size 80x80x80. Starting η = 0.1, epochs= 40.

Figure 4.1 shows the training and validation loss functions of the CAE model 1 trained with 80x80x80 size images for 40 epochs. The initial learning rate used when training this model is 0.1 and it is reduced when validation loss has stopped improving (this function is called *Reduce Learning Rate on Plateau*). As can be seen in Figure 4.1, the model did not converge after 40 epochs, but due to the computational cost of the training and the non-significant improvement in the training loss and validation loss, which was monitored by TensorBoard[1], it was not worth continuing the training for longer.

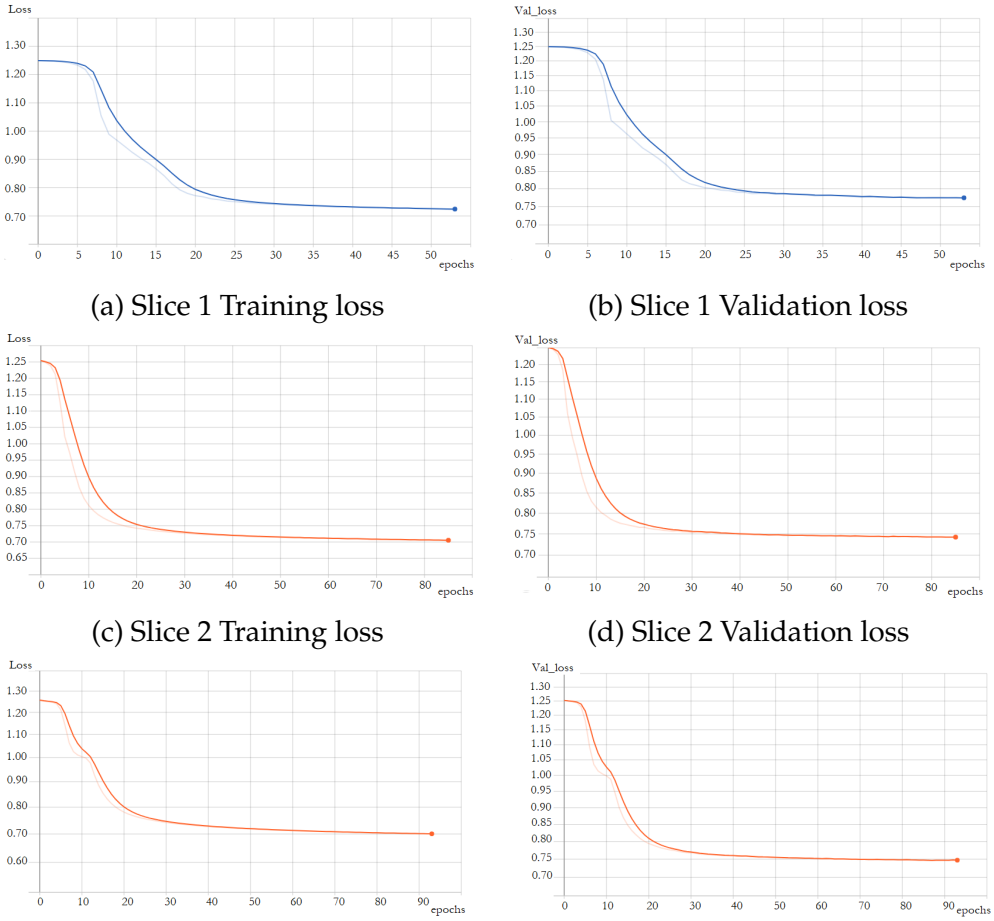

(a) Slice 1 Training loss

(b) Slice 1 Validation loss

(c) Slice 2 Training loss

(d) Slice 2 Validation loss

(e) Slice 3 Training loss

(f) Slice 3 Validation loss

Figure 4.2: Training and validation loss of the three CAE models with the three 2D slices over each dimension as input. Starting η = 0.1, epochs= 120.

[1]Visualizing learning tool of Tensorflow [60]

Figure 4.2 shows the training loss and validation loss functions of the other three CAE models which are trained with 2D images of size 80x80 for 120 epochs. The initial learning rate is the same as in the 3D CAE, and it also uses the function *Reduce Learning Rate on Plateau* and early stopping with the validation loss as metric for both cases.
As shown in Figure 4.2, the three models have similar loss curves and they converge before the 120 epochs.
Once the models are trained, manifold visualization of the reduced data is done by using t-SNE in order to see if the main 3 classes (AD, CN and MCI) of patients become separable. Figure 4.3 shows the 2-dimensional representation of the reduced data by CAE 2D trained on images from slice 1 (X and Y dimensions).

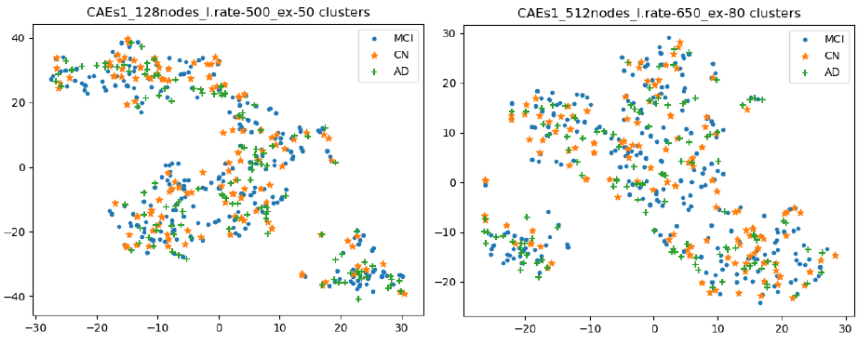

Figure 4.3: Manifold visualization of reduced data by CAE with 2D slices 1. Data was compressed into 128 nodes (left) and 512 nodes (right). On the left there is the representation of the data when reduced into 128 nodes and visualized using t-SNE parameters: *learning rate* = 500 and *early exaggeration* = 50. On the right we can see the representation of the data when reduced into 512 nodes and visualized with t-SNE parameters: *learning rate* = 650 and *early exaggeration* = 80.

Figure 4.4 shows the 2-dimensional representation of the reduced data by the CAE with 3D input data. As can be seen, neither the reduced data obtained from the CAE trained on 3D images nor from the CAE models trained on 2D images has led to a clear separation of the three main classes. Although the manifold visualization results are not indicative of suitable data representations obtained with CAE, agglomerative and DBSCAN clustering are performed because the data could be separable when using 128 or more dimensions. Other dimensionality techniques are used such as PCA and t-SNE. The algorithms are not

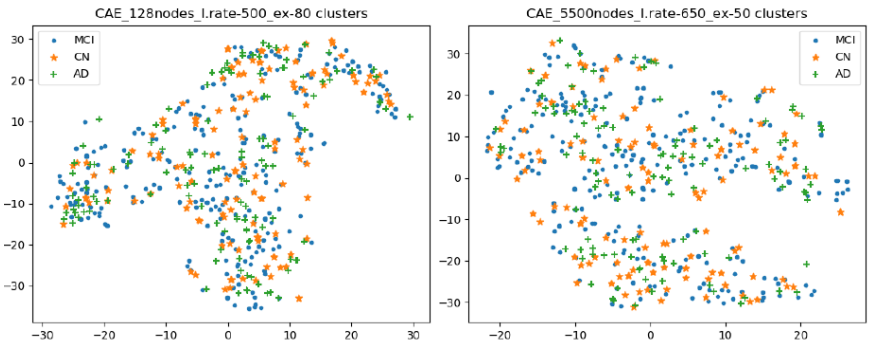

Figure 4.4: Manifold visualization of reduced data by CAE with 3D images as input. Data was compressed into 128 nodes (left) and 5500 nodes (right). On the left is presented the representation of the data when reduced into 128 nodes and visualized using t-SNE parameters: *learning rate* = 500 and *early exaggeration* = 80. On the right there is the representation of the data when reduced into 5500 nodes and visualized with t-SNE parameters: *learning rate* = 650 and *early exaggeration* = 50.

able to find the original three clusters (AD, MCI and CN) neither with the reduced data from CAE, nor reduced with the other techniques. Finally, even if it was not possible to cluster the three main groups,

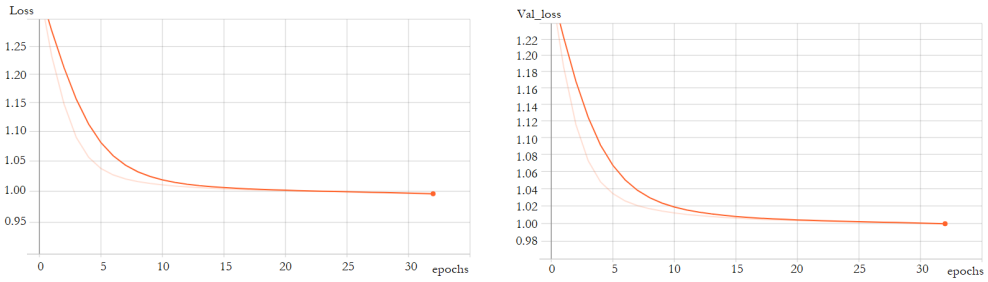

(a) Training loss (b) Validation loss

Figure 4.5: Training and validation loss functions of the CAE model 5 with input MCI images of size 80x80x80. Starting η = 0.1, epochs= 30.

CAE model 5 is trained with MCI input data which has the same parameters as the first model but uses MCI data only. It is expected that the CAE gets a better output when training with images from the same group. Figure 4.5 shows the training and validation loss functions of the CAE model 5 with 80x80x80 size MCI images for 30 epochs.

Manifold visualization is performed on the reduced data before and after applying clustering algorithms. Figure 4.6 shows the representation of the 128-dimensional compressed data by the CAE model 5. Figure 4.6(a) depicts how the six MCI clusters regarding the conversion to AD (explained in Section 3.6) are located and Figure 4.6(b) describes the representation of the clusters found by the agglomerative clustering technique. Figure 4.7 shows the same than Figure 4.6 but with 5500-dimensional compressed data.

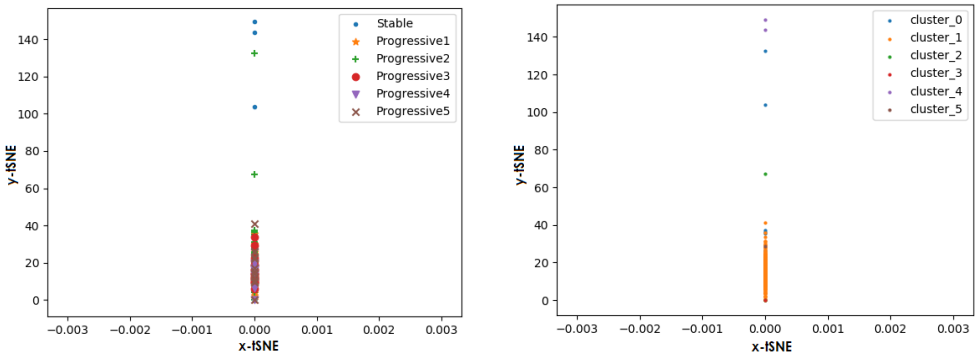

(a) MCI progression clusters (b) Found clusters

Figure 4.6: Manifold visualization of 128-dimensional data by CAE model 5 before and after applying agglomerative clustering.

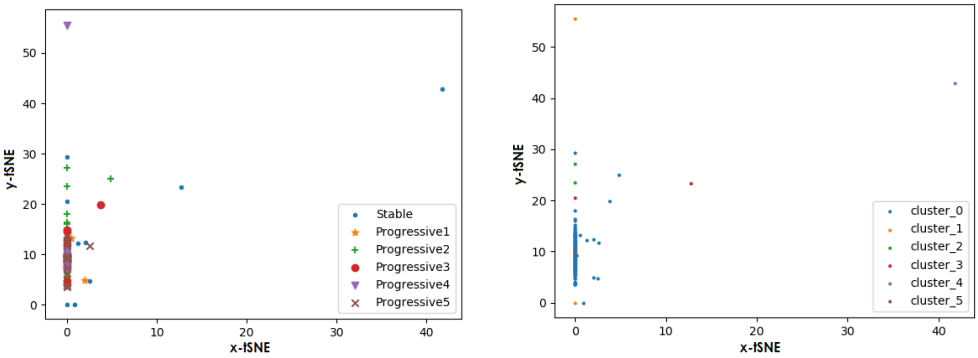

(a) MCI progression clusters (b) Found clusters

Figure 4.7: Manifold visualization of 5500-dimensional data by CAE model 5 before and after applying agglomerative clustering.

The clusters obtained by agglomerative clustering are not close to the six MCI clusters regarding the AD progression and DBSCAN cluster-

ing can just find one cluster in the data. The MCI data is rather evenly spread and it is difficult to find distinct groups.

4.2 MCI clusters regarding AD progression analysis

Using the information provided by ADNI, six clusters of MCI patients are generated as explained in Section 3.6. There is a total of 516 MCI subjects scans and they are clustered as follows: 231 *Stable MCI scans*, 78 *Progressive 1* scans, 106 *Progressive 2* scans, 44 *Progressive 3* scans, 29 *Progressive 4* scans, and 28 *Progressive 5* scans.
A comparison of image similarities is performed with the processed 3D MRI baseline scans of these six clusters. The motivation for this analysis is to examine whether at the baseline it is already possible to distinguish patients that will remain stable or develop AD at a certain time. Figure 4.8 shows the Pearson correlation matrix where the diagonal elements represent the mean of the pair-wise Pearson correlation between images of the same group and the off-diagonal elements represent the mean of the pair-wise Pearson correlation of images from two different groups.

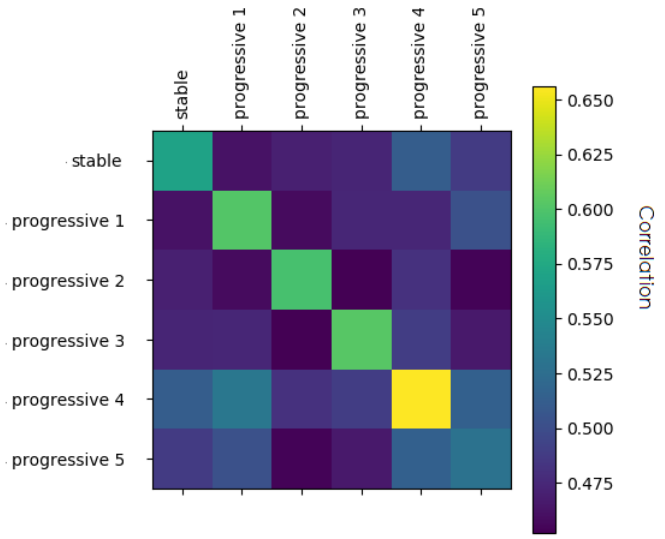

Figure 4.8: Pearson matrix correlation of stable, progressive 1, progressive 2, progressive 3, progressive 4 and progressive 5 clusters.

As expected, the diagonal values are higher than the off-diagonal values. This indicates that there are some differences, although small, in the images at the baseline that could help to cluster patients into different MCI subtypes regarding its progression to AD.
In addition to the Pearson correlation measure, another test is run in order to see whether the clusters are distinct. The mean of the maximum radius of the clusters is compared to the mean of the distance between cluster centers. This empirical statistic is calculated as follows:

$$D = \frac{\frac{1}{n}\sum_{i=1}^{n} rm_i}{\frac{1}{(n-1)n/2}\sum_{i=1}^{n-1}\sum_{j=i+1}^{n} cd_{ij}} \tag{4.1}$$

where n is the number of clusters, rm_i is the maximum radius of cluster i and cd_{ij} is the distance between centers of the two clusters i and cluster j. Figure 4.9 explains *rm* and *cd* graphically.

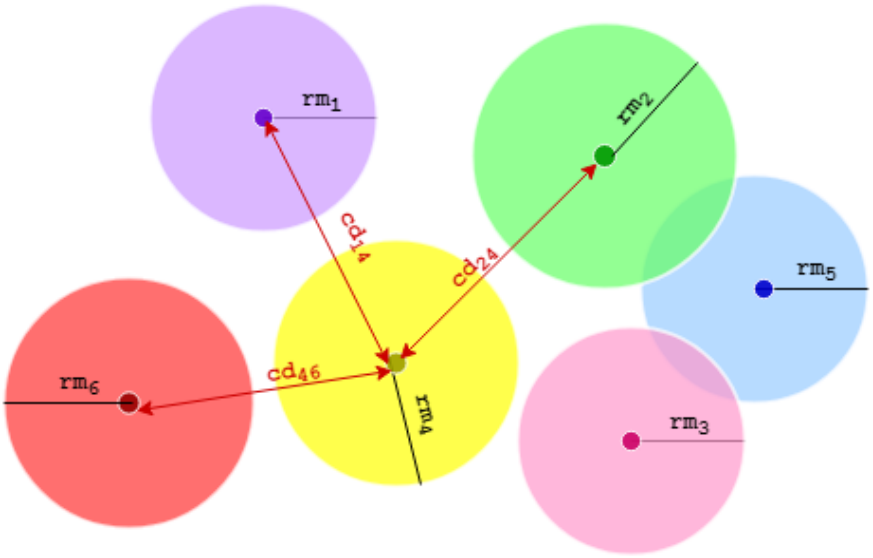

Figure 4.9: *rm* and *cd* measures from six clusters.

This difference D is calculated for the six original clusters and it is repeated 100 times for random clusters in the spirit of the random permutation test. $D_{original}$ is 3.19 while the mean of the 100 D_{random} is 3.91. Moreover $D_{original}$ is smaller than D_{random} for the 100 random cases with a difference margin = 0.1 and probability = 93%, and with a difference margin = 0.5 and probability = 71%.

The results obtained with this test indicate that the spread of each cluster is larger when they are random and that the distance between clusters is smaller, due to the proximity of the new random clusters. Since the D value of the comparison is larger than 1 we know that the radii of the clusters are larger than the distances between cluster centroids.

Chapter 5

Discussion

Throughout this work an analysis of the potential of machine learning and deep learning applied to the field of neuroimaging has been evaluated. This analysis has been conditioned to the main assumption of working with data processed as little as possible, thus avoiding expert knowledge on brain image pre-processing. The aim of the analysis was to increase the understanding of AD biomarkers in early stages, in concrete MCI subtypes. Despite intensive investigations into data representations including various approaches to dimensionality reduction I could not find clearly separable clusters based on sMRI data with machine learning.

An important question that has arisen in the project is concerned with the evaluation of the results of unsupervised learning. In the context of this research, it relates to both the autoencoder representations and clustering outcomes. It is not clear how to determine whether CAE performed well as a dimensionality reduction and feature extraction approach. Similarly, an identification of meaningful clusters in MCI data could either depend on the CAE's performance or the intrinsic differences in MRI recordings for different MCI subtypes.

Although MCI clusters found by clustering following the data dimensionality reduction were not representative, observed meaningful correlation with the baseline images of different MCI progression groups based on information provided by ADNI is found. This observation is in line with Yaffe et al.'s work in [21] where an association between the conversion to different dementia and prior subtype of MCI was found, which inspired the main question in this thesis.

The measure D described in Section 4.2 has scaling problems when using different amount of clusters. However, in this study a fixed number of six clusters is used, thus the aforementioned scaling problem does not have any effect on the outcome. Another similar measure that could have been used to analyze the clusters generated is Davies Bouldin index (DBI) [61], a cluster similarity indication. This measure accounts for dispersion of a cluster and dissimilarity between clusters [62]. Nevertheless, DBI offers a paired comparison of clusters whilst with the measure proposed in this work the general similarities are analyzed without focusing on specific clusters.
In this work a convolutional autoencoder was chosen as an unsupervised learning method for dimensionality reduction as it has proven useful in previous work in the area of AD diagnosis. However, there are other alternatives that could be considered such as Self-organizing map (SOM) [63], which produces a low-dimensional topographical representation of the data based on a specific similarity measure.

5.1 Problems and limitations

Several problems have occurred during the execution of this work and there have been some limitations that have had an impact on the result of this research, they are the following:

- The evaluation of CAE's performance was not easy. Based on the performance when using AD and CN patients data in addition to MCI, I can see that it is not good enough to extract features from MRI images processed as described in Chapter 3. Its manifold representation is not comparable to manifold representation done in Hosseini et al.'s work [15] where generic features capturing AD biomarkers are learnt from using a similar structure of CAE with bigger 3D images. However, in that case CAEs convolutional filters had to be pre-trained with carefully pre-processed data.

- As expected at the beginning of the work, the small number of images available has been a limitation when working with a deep learning approach. Nevertheless, data augmentation was studied but due to rather poor performance of the CAE and the large volume of the generated data, this technique was discarded.

- Another limitation was to train and test the model with PDC due to the long queuing time. It would have been much easier to have GPU resources just for this project and not shared with so many users.

5.2 ML on raw data vs processed MRI data

In the light of these difficulties, I have hypothesized lack of domain-specific sMRI processing, planned in this work, could be a deciding factor about my negative findings. I strongly believe that it is still interesting to explore MCI subtypes, however with carefully processed data since the atrophy differences of amnestic and non-amnestic MCI types by structural MRI have been demonstrated in [41].
While most of the work done for diagnosis and prognosis of AD uses domain-specific pre-processed sMRI data [5, 6, 7, 13], Liu et al. [9], motivated by the success of CNN in image classification, used a Cascaded CNN to learn multi-level and multimodal features of MRI and PET brain images for AD classification avoiding then this specific pre-processing.

5.3 Ethical, Societal and Sustainability aspects

There is a enormous ethical and social responsibility when working with medical data and this responsibility is assumed by ADNI in this work. ADNI provides a secure research data repository where access is controlled and patients' anonymity is ensured.
In addition, better understanding of sMRI biomarkers for detection and prediction of early stages of AD may have an important impact on successful treatments and thus on the society that suffer from this disease. As stated in [41], the assignment of MCI subtypes would be useful to improve the prediction of dementia type and the risk of conversion to dementia. Thus, for the long-term goal of this research one of the main motivations is to extend and improve the quality of life of people suffering from AD. Therefore, I believe that this work has a clear ethical component as it allocates technological resources and scientific knowledge to this purpose.

Moreover, to work with less processed data ensures saving of time and resources such as the licenses of brain imaging software.

Chapter 6

Conclusions and Future Work

The analysis done in this work did not lead to a clear answer about the likelihood of the conversion rate for any specific types of MCI since it has not been possible to find clearly separable clusters using machine learning and deep learning. However, a significant correlation within the baseline images of the respective six groups identified based on AD progression has been found which shows the possibility to identify different patterns in MCI patients sMRI scans related to the progression to AD. To the best of my knowledge, there is no previous work where MCI patients are clustered in an automated way and even less researchers working without hand-craft imaging features; thus I believe more research in this direction is necessary in order to obtain new insights to the understanding of AD biomarkers. Moreover, despite the inconclusive results, it opens a research line on using non domain-specific pre-processing in the purpose of the study of AD early stages biomarkers.

There are several aspects that could be explored in the future, such as:

- To repeat the same methodology but using properly processed images (using brain imaging software like FreeSurfer or FSL). For example to perform ROI extraction (extract the hippocampus and entorhinal) and to apply masks to the data. This is something that could be possible to do in a future collaboration with Professor Joana Pereira from the Department of Neurobiology, Care Sciences and Society (NVS) in Karolinska Institutet, which offers to share their processed data from ADNI sMRI scans for

this study.

- To use other techniques than convolutional neural networks for the feature extraction. For example try to cluster MCI patients and obtain significant discriminative features using Random forest pairwise similarity, as it is done in [64]. This also implies performing a domain-specific pre-processing to the data.

Bibliography

[1] S. G. Mueller, M. W. Weiner, L. J. Thal, R. C. Petersen, C. R. Jack, W. Jagust, J. Q. Trojanowski, A. W. Toga *et al.*, "Ways toward an early diagnosis in Alzheimer's disease: the Alzheimer's Disease Neuroimaging Initiative (ADNI)," *Alzheimer's & Dementia: The Journal of the Alzheimer's Association*, vol. 1, no. 1, pp. 55–66, Jul. 2005.

[2] R. C. Petersen, "Mild cognitive impairment as a diagnostic entity," *Journal of Internal Medicine*, vol. 256, no. 3, pp. 183–194, Sep. 2004.

[3] R. C. Petersen, "Mild Cognitive Impairment," *Continuum : Lifelong Learning in Neurology*, vol. 22, no. 2 Dementia, pp. 404–418, Apr. 2016.

[4] S. Haller, D. Nguyen, C. Rodriguez, J. Emch, G. Gold, A. Bartsch, K. O. Lovblad, and P. Giannakopoulos, "Individual prediction of cognitive decline in mild cognitive impairment using support vector machine-based analysis of diffusion tensor imaging data," *Journal of Alzheimer's disease: JAD*, vol. 22, no. 1, pp. 315–327, 2010.

[5] K. Nho, L. Shen, S. Kim, S. L. Risacher, J. D. West, T. Foroud, C. R. Jack, M. W. Weiner *et al.*, "Automatic Prediction of Conversion from Mild Cognitive Impairment to Probable Alzheimer's Disease using Structural Magnetic Resonance Imaging," *AMIA ... Annual Symposium proceedings. AMIA Symposium*, vol. 2010, pp. 542–546, Nov. 2010.

[6] S. G. Costafreda, I. D. Dinov, Z. Tu, Y. Shi, C.-Y. Liu, I. Kloszewska, P. Mecocci, H. Soininen *et al.*, "Automated hippocampal shape analysis predicts the onset of dementia in mild cognitive impairment," *NeuroImage*, vol. 56, no. 1, pp. 212–219, May 2011.

[7] S. F. Eskildsen, P. Coupé, V. S. Fonov, J. C. Pruessner, D. L. Collins, and Alzheimer's Disease Neuroimaging Initiative, "Structural imaging biomarkers of Alzheimer's disease: predicting disease progression," *Neurobiology of Aging*, vol. 36 Suppl 1, pp. S23–31, Jan. 2015.

[8] B. Duraisamy, J. V. Shanmugam, and J. Annamalai, "Alzheimer disease detection from structural mr images using fcm based weighted probabilistic neural network," *Brain imaging and behavior*, pp. 1–24, 2018.

[9] M. Liu, D. Cheng, K. Wang, Y. Wang, and the Alzheimer's Disease Neuroimaging Initiative, "Multi-Modality Cascaded Convolutional Neural Networks for Alzheimer's Disease Diagnosis," *Neuroinformatics*, vol. 16, no. 3-4, pp. 295–308, Oct. 2018.

[10] G. Orrù, W. Pettersson-Yeo, A. F. Marquand, G. Sartori, and A. Mechelli, "Using Support Vector Machine to identify imaging biomarkers of neurological and psychiatric disease: a critical review," *Neuroscience and Biobehavioral Reviews*, vol. 36, no. 4, pp. 1140–1152, Apr. 2012.

[11] R. Wolz, V. Julkunen, J. Koikkalainen, E. Niskanen, D. P. Zhang, D. Rueckert, H. Soininen, J. Lötjönen *et al.*, "Multi-method analysis of MRI images in early diagnostics of Alzheimer's disease," *PloS One*, vol. 6, no. 10, p. e25446, 2011.

[12] S. Lu, Y. Xia, W. Cai, M. Fulham, and D. D. Feng, "Early identification of mild cognitive impairment using incomplete random forest-robust support vector machine and FDG-PET imaging," *Computerized Medical Imaging and Graphics*, vol. 60, pp. 35–41, Sep. 2017.

[13] K. Ning, B. Chen, F. Sun, Z. Hobel, L. Zhao, W. Matloff, Alzheimer's Disease Neuroimaging Initiative, and A. W. Toga, "Classifying Alzheimer's disease with brain imaging and genetic data using a neural network framework," *Neurobiology of Aging*, vol. 68, pp. 151–158, Aug. 2018.

[14] A. Payan and G. Montana, "Predicting alzheimer's disease - a neuroimaging study with 3d convolutional neural networks." in

ICPRAM (2), M. D. Marsico, M. A. T. Figueiredo, and A. L. N. Fred, Eds. SciTePress, 2015, pp. 355–362.

[15] E. Hosseini asl, M. Ghazal, A. Mahmoud, A. Aslantas, A. Shalaby, M. F Casanova, G. Barnes, G. Gimel'farb *et al.*, "Alzheimer's disease diagnostics by a 3d deeply supervised adaptable convolutional network," *Frontiers in bioscience (Landmark edition)*, vol. 23, pp. 584–596, 01 2018.

[16] "ADNI | About." [Online]. Available: http://adni.loni.usc.edu/about/

[17] R. C. Petersen, R. O. Roberts, D. S. Knopman, Y. E. Geda, R. H. Cha, V. S. Pankratz, B. F. Boeve, E. G. Tangalos *et al.*, "Prevalence of mild cognitive impairment is higher in men. The Mayo Clinic Study of Aging," *Neurology*, vol. 75, no. 10, pp. 889–897, Sep. 2010.

[18] B. Lorensen, "The ICBM (International Consortium for Brain Mapping) single subject brain atlas.: lorensen/ICBMBrainAtlas," Feb. 2017, original-date: 2015-02-18T15:15:29Z. [Online]. Available: https://github.com/lorensen/ICBMBrainAtlas

[19] D. Purves, Ed., *Neuroscience*, 3rd ed. Sunderland, Mass: Sinauer Associates, Publishers, 2004.

[20] D. Dickson and R. O. Weller, *Neurodegeneration: the molecular pathology of dementia and movement disorders*. John Wiley & Sons, 2011.

[21] K. Yaffe, R. C. Petersen, K. Lindquist, J. Kramer, and B. Miller, "Subtype of mild cognitive impairment and progression to dementia and death," *Dementia and Geriatric Cognitive Disorders*, vol. 22, no. 4, pp. 312–319, 2006.

[22] M. Larobina and L. Murino, "Medical Image File Formats," *Journal of Digital Imaging*, vol. 27, no. 2, pp. 200–206, Apr. 2014.

[23] E. Gibson, W. Li, C. Sudre, L. Fidon, D. I. Shakir, G. Wang, Z. Eaton-Rosen, R. Gray *et al.*, "NiftyNet: a deep-learning platform for medical imaging," *Computer Methods and Programs in Biomedicine*, vol. 158, pp. 113–122, May 2018.

[24] W. D. Bidgood, S. C. Horii, F. W. Prior, and D. E. Van Syckle, "Understanding and using DICOM, the data interchange standard for biomedical imaging," *Journal of the American Medical Informatics Association: JAMIA*, vol. 4, no. 3, pp. 199–212, Jun. 1997.

[25] R. A. Robb, D. P. Hanson, R. A. Karwoski, A. G. Larson, E. L. Workman, and M. C. Stacy, "Analyze: a comprehensive, operator-interactive software package for multidimensional medical image display and analysis," *Computerized Medical Imaging and Graphics: The Official Journal of the Computerized Medical Imaging Society*, vol. 13, no. 6, pp. 433–454, Dec. 1989.

[26] "NIfTI documentation." [Online]. Available: https://nifti.nimh.nih.gov/pub/dist/src/niftilib/nifti1.h

[27] "MINC software library and tools." [Online]. Available: http://www.bic.mni.mcgill.ca/ServicesSoftware/MINC

[28] S. Teipel, A. Drzezga, M. J. Grothe, H. Barthel, G. Chételat, N. Schuff, P. Skudlarski, E. Cavedo *et al.*, "Multimodal imaging in Alzheimer's disease: validity and usefulness for early detection," *The Lancet. Neurology*, vol. 14, no. 10, pp. 1037–1053, Oct. 2015.

[29] E. M. Haacke, R. W. Brown, M. R. Thompson, R. Venkatesan *et al.*, *Magnetic resonance imaging: physical principles and sequence design*. Wiley-Liss New York:, 1999, vol. 82.

[30] R. Frackowiak and K. Friston, "Functional neuroanatomy of the human brain: positron emission tomography–a new neuroanatomical technique." *Journal of Anatomy*, vol. 184, no. Pt 2, p. 211, 1994.

[31] A. L. Alexander, J. E. Lee, M. Lazar, and A. S. Field, "Diffusion tensor imaging of the brain," *Neurotherapeutics*, vol. 4, no. 3, pp. 316–329, 2007.

[32] K. Strimbu and J. A. Tavel, "What are Biomarkers?" *Current opinion in HIV and AIDS*, vol. 5, no. 6, pp. 463–466, Nov. 2010.

[33] W. H. Organization *et al.*, "Biomarkers in risk assessment: Validity and validation," 2001.

[34] "Consensus report of the Working Group on: "Molecular and Biochemical Markers of Alzheimer's Disease". The Ronald and Nancy Reagan Research Institute of the Alzheimer's Association and the National Institute on Aging Working Group," *Neurobiology of Aging*, vol. 19, no. 2, pp. 109–116, Apr. 1998.

[35] E. G. Kehoe, J. P. McNulty, P. G. Mullins, and A. L. W. Bokde, "Advances in MRI biomarkers for the diagnosis of Alzheimer's disease," *Biomarkers in Medicine*, vol. 8, no. 9, pp. 1151–1169, 2014.

[36] I. Goodfellow, Y. Bengio, and A. Courville, *Deep Learning*. MIT press, 2016.

[37] K. P. Murphy, *Machine Learning: A Probabilistic Perspective*. The MIT Press, 2012.

[38] L. v. d. Maaten and G. Hinton, "Visualizing data using t-sne," *Journal of machine learning research*, vol. 9, no. Nov, pp. 2579–2605, 2008.

[39] M. Ester, H.-P. Kriegel, J. Sander, and X. Xu, "Density-based spatial clustering of applications with noise," in *Int. Conf. Knowledge Discovery and Data Mining*, vol. 240, 1996.

[40] P. Fischer, S. Jungwirth, S. Zehetmayer, S. Weissgram, S. Hoenigschnabl, E. Gelpi, W. Krampla, and K. H. Tragl, "Conversion from subtypes of mild cognitive impairment to Alzheimer dementia," *Neurology*, vol. 68, no. 4, pp. 288–291, Jan. 2007.

[41] G. Csukly, E. o. Sirály, Z. Fodor, A. Horváth, P. Salacz, Z. Hidasi, E. Csibri, G. Rudas *et al.*, "The Differentiation of Amnestic Type MCI from the Non-Amnestic Types by Structural MRI," *Frontiers in Aging Neuroscience*, vol. 8, Mar. 2016.

[42] M. Jenkinson, C. F. Beckmann, T. E. Behrens, M. W. Woolrich, and S. M. Smith, "Fsl," *Neuroimage*, vol. 62, no. 2, pp. 782–790, 2012.

[43] B. Fischl, "Freesurfer," *Neuroimage*, vol. 62, no. 2, pp. 774–781, 2012.

[44] S. B. Eickhoff, K. E. Stephan, H. Mohlberg, C. Grefkes, G. R. Fink, K. Amunts, and K. Zilles, "A new spm toolbox for combining probabilistic cytoarchitectonic maps and functional imaging data," *Neuroimage*, vol. 25, no. 4, pp. 1325–1335, 2005.

[45] D. Shen, G. Wu, and H.-I. Suk, "Deep Learning in Medical Image Analysis," *Annual review of biomedical engineering*, vol. 19, pp. 221–248, Jun. 2017.

[46] H.-C. Shin, M. R. Orton, D. J. Collins, S. J. Doran, and M. O. Leach, "Stacked autoencoders for unsupervised feature learning and multiple organ detection in a pilot study using 4d patient data," *IEEE transactions on pattern analysis and machine intelligence*, vol. 35, no. 8, pp. 1930–1943, Aug. 2013.

[47] J. Kleesiek, G. Urban, A. Hubert, D. Schwarz, K. Maier-Hein, M. Bendszus, and A. Biller, "Deep MRI brain extraction: A 3d convolutional neural network for skull stripping," *NeuroImage*, vol. 129, pp. 460–469, Apr. 2016.

[48] W. Zhang, R. Li, H. Deng, L. Wang, W. Lin, S. Ji, and D. Shen, "Deep convolutional neural networks for multi-modality isointense infant brain image segmentation," *NeuroImage*, vol. 108, pp. 214–224, Mar. 2015.

[49] S. Pereira, A. Pinto, V. Alves, and C. A. Silva, "Brain Tumor Segmentation Using Convolutional Neural Networks in MRI Images," *IEEE transactions on medical imaging*, vol. 35, no. 5, pp. 1240–1251, 2016.

[50] "ADNI | MRI Analysis." [Online]. Available: http://adni.loni.usc.edu/methods/mri-tool/mri-analysis/

[51] S. M. Smith, "Fast robust automated brain extraction," *Human Brain Mapping*, vol. 17, no. 3, pp. 143–155, Nov. 2002.

[52] M. Brett, M. Hanke, B. Cipollini, M.-A. Côté, C. Markiewicz, S. Gerhard, E. Larson, G. R. Lee *et al.*, "nibabel: 2.1. 0," *Zenodo*, 2016.

[53] C. Rorden, L. Bonilha, J. Fridriksson, B. Bender, and H.-O. Karnath, "Age-specific ct and mri templates for spatial normalization," *Neuroimage*, vol. 61, no. 4, pp. 957–965, 2012.

[54] F. Pedregosa, G. Varoquaux, A. Gramfort, V. Michel, B. Thirion, O. Grisel, M. Blondel, P. Prettenhofer *et al.*, "Scikit-learn: Machine learning in Python," *Journal of Machine Learning Research*, vol. 12, pp. 2825–2830, 2011.

[55] S. Toor, M. Lindberg, I. Falman, A. Vallin, O. Mohill, P. Freyhult, L. Nilsson, M. Agback *et al.*, "Snic science cloud (ssc): A national-scale cloud infrastructure for swedish academia," in *2017 IEEE 13th International Conference on e-Science (e-Science)*. IEEE, 2017, pp. 219–227.

[56] "PDC documentation." [Online]. Available: https://www.pdc.kth.se/about/what-is-pdc-1.736889

[57] F. Chollet *et al.*, "Keras," 2015.

[58] M. Abadi, P. Barham, J. Chen, Z. Chen, A. Davis, J. Dean, M. Devin, S. Ghemawat *et al.*, "Tensorflow: A system for large-scale machine learning," in *12th {USENIX} Symposium on Operating Systems Design and Implementation ({OSDI} 16)*, 2016, pp. 265–283.

[59] M. Holden, D. Hill, E. Denton, J. Jarosz, T. C. S. Cox, T. Rohlfing, J. Goodey, and D. J. Hawkes, "Voxel similarity measures for 3d serial mr brain image registration." *IEEE Trans. Med. Imaging*, vol. 19, pp. 94–102, 01 2000.

[60] D. Mané *et al.*, "Tensorboard: Tensorflow's visualization toolkit, 2015."

[61] D. L. Davies and D. W. Bouldin, "A cluster separation measure," *IEEE transactions on pattern analysis and machine intelligence*, no. 2, pp. 224–227, 1979.

[62] S. Saitta, B. Raphael, and I. F. Smith, "A bounded index for cluster validity," in *International Workshop on Machine Learning and Data Mining in Pattern Recognition*. Springer, 2007, pp. 174–187.

[63] T. Kohonen, "The self-organizing map," *Proceedings of the IEEE*, vol. 78, no. 9, pp. 1464–1480, 1990.

[64] K. Poulakis, J. B. Pereira, P. Mecocci, B. Vellas, M. Tsolaki, I. Kłoszewska, H. Soininen, S. Lovestone *et al.*, "Heterogeneous

patterns of brain atrophy in Alzheimer's disease," *Neurobiology of Aging*, vol. 65, pp. 98–108, 2018.